PROJECT FINAL REPORT
PUBLISHABLE SUMMARY

Grant Agreement number:	**(FP7-ICT-2007-2) - 224366**
Project acronym:	**DELIGHT**
Project title:	**Development of low-cost technologies for the fabrication of high-performance telecommunication lasers**
Funding Scheme:	**CP – FP**
Period covered:	from **01.09.2008** to **31.07.2012**

Name of the scientific representative of the project's co-ordinator: **Mihail Dumitrescu**

|	
Title:	**Adj. Prof. / Docent**
Organisation:	**Tampere University of Technology,**
	Optoelectronics Research Centre
Tel:	**+358 50 348 6408**
Fax:	**+358 3 364 1436**
E-mail:	**Mihail.Dumitrescu@tut.fi**
Project website address:	**http://www.delightproject.eu/**

Contents

Executive summary

The DeLight project was aimed at developing low-cost high-performance telecommunication lasers by employing advanced laser structures and fabrication technologies. Three critical elements were addressed in terms of reducing the fabrication cost of the lasers:

- the difficulty and complexity of the fabrication;
- the cost of equipment ownership and the fabrication process throughput;
- the fabrication yield and the controllability of the device characteristics.

Laterally-coupled (or laterally-corrugated) ridge waveguide (LC-RWG) surface gratings, illustrated in Fig. 1a and 1b, have been developed to avoid the problematic overgrowth employed in the fabrication of conventional buried gratings, thus reducing the fabrication difficulty and complexity. The cost of equipment ownership and the fabrication throughput were addressed by employing UV nanoimprint lithography for imprinting the fabrication process masks. Etched end facets, fabricated in conjunction with the LC-RWG surface gratings (Fig. 1b), have been developed and tested for improving the fabrication yield and the device performances, which are largely influenced by the uncontrollable positions of the cleaved end facets.
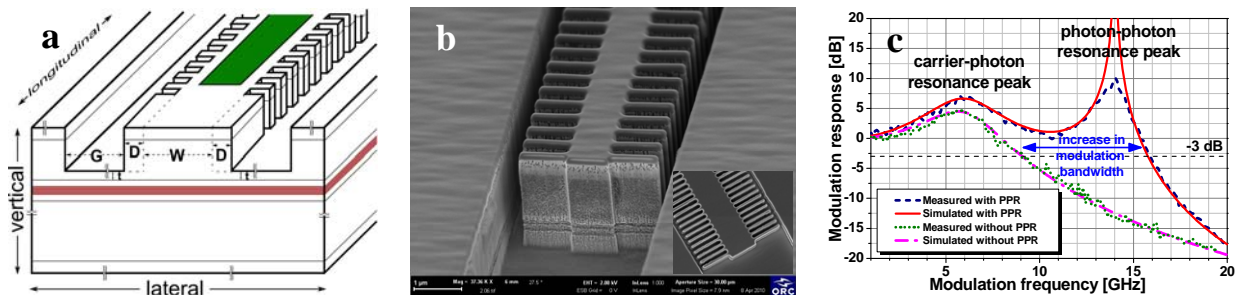
Fig. 0-1: a) Sketch of the laterally-coupled ridge-waveguide (LC-RWG) grating structure; b) SEM images of the etched facet of a laser with LC-RWG gratings; c) measured and simulated small-signal modulation responses from DFB lasers with and without PPR.

In terms of improving the performances of telecommunication lasers the main target was on increasing the laser direct modulation bandwidth. It should be noted that, despite considerable research efforts, the direct laser modulation bandwidth has improved much less than the other laser characteristics. This is mainly because it has conventionally been linked to the carrier-photon resonance (CPR), which has inherent physical limitations. Consequently, DeLight did not target the increase in direct modulation bandwidth by increasing the CPR but by introducing a supplementary high-frequency photon-photon resonance (PPR). Fig. 1c shows the simulated and measured small-signal modulation responses for two types of lasers with different longitudinal structures, which were fabricated in the same fabrication run from the same 'legacy' epiwafer (intended for the fabrication of Fabry-Perot lasers at 1.55 µm). The figure illustrates the increase in direct amplitude-modulation bandwidth by comparing the modulation response of a single-section distributed feedback (DFB) laser that does not have PPR with the modulation response of a multi-section laser with the PPR properly placed with respect to the CPR.

Multi-section lasers employing LC-RWG surface gratings and operating at 1.3 and 1.55 µm have been designed, fabricated (mainly from legacy epiwafers, intended for Fabry-Perot lasers) and characterized. Photon-photon resonances, largely determined by the longitudinal structure of the lasers and adjustable by bias, were achieved consistently and systematically, according to the model and simulations. The project was successful in developing the LC-RWG surface gratings combined with a UV-NIL-based cost-effective fabrication process and a new concept for extending the direct laser modulation bandwidth by exploiting the PPR. However, due to the combined complexity of the technical problems to be solved, in particular due to the difficulty of achieving a relatively smooth and controllable small-signal modulation response between the CPR and the PPR (mainly when those are spaced far apart), the project fell short of achieving its final quantitative goal: a low-cost direct modulated laser capable of 43 Gbit/s. However, the results obtained by DeLight prove that there is a definite possibility for fabricating low-cost high-performance telecommunication lasers by exploiting LC-RWG surface gratings, nanoimprint lithography and the photon-photon resonance.

1. Summary description of project context, objectives and structure

The optical communication laser market size was roughly 2.3 billion dollars in 2012, with strong growth expected, especially for the high-speed domain, as the capacity demand is being driven by the increased use of smart phones and by the video streaming services' popularity. At present the fastest optical transmissions are achieved with lasers externally modulated by electro-optic modulators. However, these have several disadvantages when compared with directly-modulated lasers: they have a higher complexity, consume more power, have a larger footprint, require more cooling and ultimately incur greater costs. In spite of all their disadvantages, the externally modulated lasers are still widely used in high-speed applications, mainly because the directly-modulated lasers are simply not fast enough. The conventional limitation of the direct modulation speed is given by the carrier-photon resonance (CPR), which, being derived from the carrier and photon lifetimes, cannot be pushed too high without detrimentally affecting the laser performance as a light source.

Taking into account the physical limitations imposed on the increase of the CPR, the DeLight project targeted the increase in the laser direct modulation speed by introducing one (or more) supplementary resonant frequencies above the CPR. These supplementary resonances are placed at frequencies corresponding to the frequency difference between two quasi-phase-locked optical modes of the laser cavity. This is why they are called photon-photon resonances (PPRs). By properly favoring two or more quasi-phase-locked cavity modes and adding the corresponding supplementary photon-photon resonances to the laser we enable it to be modulated much faster.

The high-speed optical transmission applications (e.g. 100 Gb Ethernet, optical connections in supercomputer clusters and data farms, etc.) require a large number of lasers and put a premium on low cost. Consequently, DeLight has investigated and addressed the main elements that influence the cost of the high-speed directly-modulated lasers: the difficulty and complexity of the fabrication, the cost of equipment ownership, the fabrication process throughput and the fabrication yield (including the controllability/reproducibility of the device characteristics).

The conventional buried-grating distributed feedback (DFB) lasers (based on embedding the grating deep into the epilayer structure) require two or more epitaxial growth steps, complicating the fabrication, affecting the device performance, yield and reliability (especially when Al-containing materials are used) and, ultimately, increasing the device cost. To avoid the problematic overgrowth we have employed laterally-coupled (laterally-corrugated) ridge-waveguide (LC-RWG) surface gratings, illustrated in Fig. 2, which are applicable to different materials, including Al-containing ones, and can be easily integrated in complex device structures and photonic circuits. A supplementary advantage of the LC-RWG gratings derives from the fact that there is only a limited interaction between the defect-prone processed grating interfaces and the carriers, which leads to more stable devices with better performances and increased reliability.
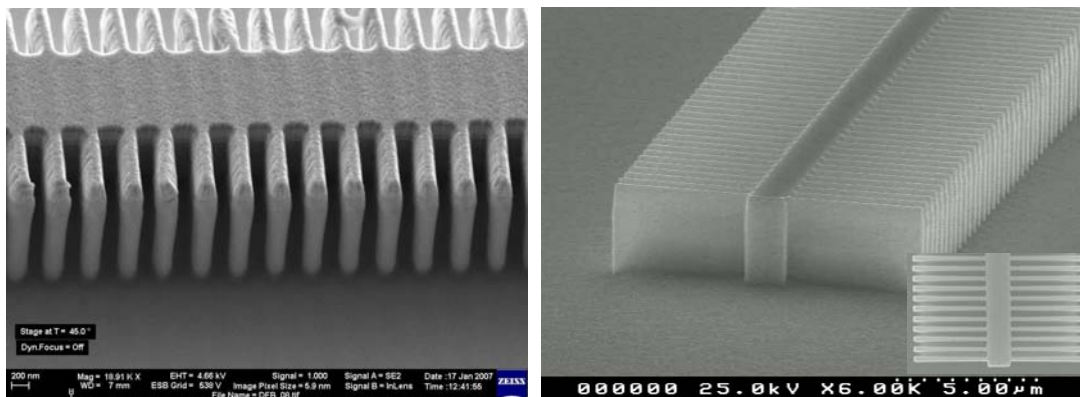
Fig. 1-1: (a) Scanning electron microscopy (SEM) close-up of LC-RWG surface gratings; (b) SEM images of the end section of a DFB laser with LC-RWG surface gratings and etched end facet.

The dimensions of the LC-RWG grating features (in the hundred nanometer range on the longitudinal direction, which is a thousand times smaller than the diameter of human hair) require advanced lithographic techniques for imprinting the etching masks. Moreover the grating structure in multi-section devices is not periodic along the whole device length. Accordingly, the only usable conventional projection lithographic technique is the electron beam lithography (EBL). This lithographic technique requires very expensive

DELIGHT
*Development of low-cost technologies for the fabrication
of high-performance telecommunication lasers*

equipment for imprinting the mask sizes required by the processing of the LC-RWG gratings and is a slow (and costly) serial procedure. Consequently, in DeLight we have developed a cost-effective fabrication procedure based on UV-nanoimprint lithography (UV-NIL), which has several significant advantages:

- capability of full-wafer scale imprint with resolutions below 10 nm,
- flexibility in imprinting complex (longitudinally non-periodic) structures,
- equipment cost of ownership substantially smaller than for EBL,
- small cost for consumable materials,
- high throughput (~1000 wafers / week with non-automated/manual operation).

An important element in determining the device cost is the fabrication yield, which is related to how many of the fabricated devices achieve the target characteristics. For the DFB lasers the yield is significantly affected by the incontrollable position of the cleaved end facets with respect to the gratings. Although good anti-reflection coatings of the cleaved end facets mitigate the effect of the incontrollable phase of the end-facet reflections for DFB lasers with high coupling coefficient buried gratings, in the case of lower coupling coefficient surface gratings, the phase matching of the end-facet reflections with the grating reflection is highly beneficial for stabilizing the device characteristics and improving the fabrication yield. Therefore, we have developed and tested etched facets in conjunction with the LC-RWG surface gratings (Fig. 2b).

The project had two main objectives:
(a) The development of high-performance surface-grating-based DFB/DBR telecom lasers
(b) The development of ultra-high speed directly modulated lasers (> 28 Gbit/s intermediate target and > 43 Gbit/s final target) with a simplified multi-section design, which exploit high-order photonic resonances for extending the modulation bandwidth.

The most important quantitative target performance of the project was the modulation bandwidth. Since the standardization for the next transceiver generation aims for handling a transmission rate of 100 Gbit/s with a CFBI (*C = 100 Gbit/s; F = four; B = bit; I = interface*) 4 x 25 Gbit/s interface, the intermediate target datarate (including overhead transmission for all envisioned applications) was 28 Gbit/s (which means a small-signal bandwidth > 21 GHz). This intermediate target datarate was extended to 43 Gbit/s as the final quantitative goal of the project in terms of direct laser modulation bandwidth (since the longer term transceiver development is aiming at a serial transmission rate of 40 Gbit/s, i.e. 43 Gbit/s with overhead transmission).

Another important objective was to develop a common technological fabrication platform, based on surface gratings and supported by cost-effective UV nanoimprint lithography (UV-NIL). The surface-oriented technology should be applicable even to 'legacy' epilayer structures intended for the fabrication of Fabry-Perot lasers, thus enabling the fabrication of higher-performance lasers from already tested and qualified, less complex and cheaper 'legacy' epiwafers.

The DeLight Consortium comprises six academic research partners - the Optoelectronics Research Centre of the Tampere University of Technology, the Institute of Nanostructure Technologies and Analytics of the University of Kassel, the Chair of Applied Physics (Technische Physik) of the University of Wurzburg, the Department of Electronics of Politecnico di Torino , the Electrical Engineering Department of the Israel Institute of Technology, and the Institute of Physics of the Wroclaw University of Technology - one private research organization - III-V Lab of Alcatel-Thales - and two SMEs – Modulight Inc. and ColorChip Ltd. - representing a total of five European countries - Finland, Germany, Italy, France, Poland – and one EU associated country – Israel. The partners' abbreviated names and primary activities within DeLight are given in Table 1-1.

The work in DeLight has been organized in eight workpackages (WPs):
- WP1a Project Management
- WP1b Scientific coordination
- WP2   Modeling, simulation and design
- WP3   Development of growth technology and epiwafer growth
- WP4   Development of device processing technologies
- WP5   Packaging and module development
- WP6   Material, device and module characterization

- WP7   Dissemination and exploitation

Nr.	Organization	Abrev. (Type of org.)	Country	Primary activities	Principal investigator (E-mail address)
1	Optoelectronics Research Centre, Tampere University of Technology	ORC-TTY (Univ.)	Finland	Modeling, simulation and design, epitaxial growth (QW), device processing, nanoimprint lithography, material and device characterization	Adj. Prof. Mihail Dumitrescu (Mihail.Dumitrescu@tut.fi)
2	Institute of Nano-structure Technologies and Analytics, Universität Kassel	UKAS (Univ.)	Germany	Epitaxial growth (QD/QDash), device processing, e-beam lithography, material and device characterization	Prof. Johann-Peter Reithmaier (jpreith@ina.uni-kassel.de)
3	Technische Physik, Universität Würzburg	UWUERZ (Univ.)	Germany	Epitaxial growth (QW), device processing, e-beam lithography, material and device characterization	Prof. Martin Kamp (Martin.Kamp@physik.uni-wuerzburg.de)
4	Dept. of Electronics, Politecnico di Torino	PT (Univ.)	Italy	Modeling, simulation and design	Prof. Ivo Montrosset (Ivo.Montrosset@polito.it)
5	III-V Lab, Alcatel-Thales	III-V Lab (Comp.)	France	Epitaxial growth (QW), device processing,, material and device characterization	Dr. Olivier Parillaud (Olivier.Parillaud@3-5lab.fr)
6	Electrical Engineering Dept, Israel Institute of Technology	TN (Univ.)	Israel	Modeling, simulation and design, advanced high-speed characterization	Prof. Gadi Eisenstein (Gad@ee.technion.ac.il)
7	Modulight Inc.	Modu (SME)	Finland	Legacy epiwafer growth (QW), device characterization, burn-in, lifetest	Dr. Petteri Uusimaa (Petteri.Uusimaa@modulight.com)
8	~~MergeOptics GmbH~~ (left the consortium during the second project period)	Merge (SME)	Germany	Device specifications, module design, development of driver IC and package, TOSA and module assembly, module characterization	~~Dr. Klaus Schulz~~
8bis	ColorChip Ltd. (joined the consortium for the third project period, replacing MergeOptics)	CC (SME)	Israel	Module design, driver IC implementation and device packaging, module characterization	Dr. David Brooks (Brooks@color-chip.com)
9	Institute of Physics, Wroclaw University of Technology	WrUT (Univ.)	Poland	Advanced / microscopic material characterization	Dr. Grzegorz Sek (Grzegorz.Sek@pwr.wroc.pl)

Table 1-1: The DeLight partners, including their primary technical contributions to the project.

Workpackage	WP Director	Leader Organisation
WP1a Project Management	Adj.Prof. M. Dumitrescu	TTY
WP1b Scientific coordination	Prof. J.P. Reithmaier	UKAS
WP2 Modeling, simulation and design	Prof. Ivo Montrosset	PT
WP3 Development of growth technology and epiwafer growth	Prof. Martin Kamp	UWUERZ
WP4 Development of device processing technologies	Prof. J.P. Reithmaier	UKAS
WP5 Packaging and module development	(~~Dr. Klaus Schulz~~) Dr. David Brooks	(~~Merge~~) CC
WP6 Material, device and module characterization	Prof. Gadi Eisenstein	TN
WP7 Dissemination and exploitation	Dr. Michel Krakowski	III-V Lab

Table 1-2: List of Workpackages with their directors and leader organizations

The project duration was 47 months (from 01.09.2008 to 31.07.2012), divided into three periods:
- ➢ Period 1, 12 months, from 01.09.2008 to 31.08.2009;
- ➢ Period 2, 12 months, from 01.09.2009 to 31.08.2010;
- ➢ Period 3, 12 months plus an extension of 11 months, from 01.09.2010 to 31.07.2012.

DELIGHT
Development of low-cost technologies for the fabrication
of high-performance telecommunication lasers

2. Main scientific and technical/technological results

The scientific and technical/technological results of the project have been obtained in the workpackages from WP2 to WP6, encompassing the stages of device and module development from modelling, simulation and design (WP2) to epitaxial growth (WP3), device processing (WP4), package and module development (WP5) and device and module characterization (WP6). An overview of the main achievements is given in section 2.1, followed by more detailed description of the achievements for each of the project workpackages.

2.1. Overview of main project achievements

✓ the project developed the understanding and modeling of laterally-coupled ridge-waveguide (LC-RWG) surface gratings and performed extensive simulation studies supporting their development and fabrication;

✓ the project developed the understanding and modeling of the photon-photon resonance (PPR) effect and performed simulation studies to support the development and fabrication of three types of lasers exhibiting PPR: coupled-cavity injection grating lasers, multi-section distributed feedback lasers and distributed Bragg reflector lasers;

✓ a ultra-violet nanoimprint lithography (UV-NIL) process was developed, which enables the imprinting of process masks for the fabrication of LC-RWG gratings at telecom wavelengths down to 1st order with high throughput;

✓ UV-NIL-compatible, LC-RWG grating fabrication processes, enabling high grating coupling coefficients, were successfully developed for GaAs-based (at 1.3 μm) and InP-based (at 1.3 and 1.55 μm) lasers;

✓ fundamental properties (as electronic structure details and carrier kinetics) have been investigated in detail for various types of active regions emitting at 1.3 and 1.55 μm, in particular GaAs-based dilute nitride quantum wells, quantum dot (QD) tunnel injection structures and InAs QD and QD-like structures, in order to improve their high-speed direct modulation capabilities;

✓ the capability to control the PPR frequency between tens of GHz up to 1 THz by laser structure and to tune it by bias adjustments has been tested;

✓ InP based DFB, DBR and multi-section lasers with PPR frequencies designed for 20 – 40 GHz, including a new two-section DBR laser design with a clear PPR bandwidth enhancement, were successfully fabricated from different types of epiwafers (including legacy epiwafers intended for high-speed Fabry-Perot lasers) with different surface grating fabrication techniques;

✓ short-cavity RWG QD lasers with record values in direct digital modulation (> 20 Gbit/s) were fabricated for the first time.

✓ 127 scientific/technical/technological contributions were published: 33 in peer review journals and 94 presented in international conferences;

✓ an international workshop on "High speed semiconductor lasers (HSSL)" was organized, with the participation of renowned experts from Europe, Japan and the United States;

✓ 4 IPR items were identified and are filed as patent or in the process of patent application filing;

✓ a detailed technology implementation plan was prepared for the exploitation of project results.

Overall the DeLight project proved the possibility to fabricate low-cost high-performance telecommunication lasers by exploiting LC-RWG surface gratings, nanoimprint lithography and by taking advantage of the photon-photon resonance to extend the direct laser modulation speed.

2.2. Achievements in WP2 "Modeling, simulation and design"

WP2 was meant to support the other workpackages and addressed the following specific objectives:

- define the system specification of laser characteristics - this objective was addressed by MergeOptics in the first period of the project;
- analyze and develop the laser epilayer structures to support LC-RWG grating implementation and high-speed operation (including the analysis of the possible exploitation of legacy epilayer structures already developed for high-speed Fabry-Perot lasers) – this objective was addressed mainly by ORC-TTY and PT with feedback from the epilayer growth and device fabrication performed at ORC-TTY, III-V Lab and UKAS; the effort towards this objective has been more sustained in the first part of the project (until it was found out that the legacy epiwafers are well suited for high-speed lasers with LC-RWG surface gratings), but continued to the end of the project for advanced epilayer structure development (like the epilayers for high-speed lasers with quantum dash and quantum dot active regions);
- develop the ridge waveguide and LC-RWG gratings to achieve the target device characteristics (in particular a good grating coupling coefficient and reduced losses) with structures compatible with a fabrication process employing nanoimprint lithography – this objective (which was aimed at finding the best structural choices within the technological limitations) was addressed by ORC-TTY and PT, largely in the first two periods of the project;
- development of the laser structure to achieve systematic and reproducible photon-photon resonance and extended direct-modulation bandwidth – this objective, which also targeted a simplified laser structure as well as a simplified control (limited number of contacts/currents) and a stable operation, was addressed by ORC-TTY and PT over the whole project duration;
- static and dynamic modeling and simulation for different distributed feedback (DFB) and distributed Bragg reflector (DBR) lasers, including multi-section lasers (comprising several gain, grating and phase-control sections) – this objective was addressed from about the end of the first period until the end of the project by ORC-TTY, PT and TN, with feedback from ORC-TTY, UKAS, UWUERZ, III-V Lab, TN, Modu and ColorChip.

The main scientific and technical results achieved in WP2 are:

- ✓ the development (done in parallel by ORC-TTY and PT) of software tools for analyzing the effect of different grating parameters (grating order, filling factor, grating trench width, ridge geometry, etching profile) on the coupling coefficient as well as on the modal behavior of DFB/DBR lasers with surface gratings;
- ✓ the development (done by ORC-TTY and PT) of numerical methods/programs to analyze, design and extract the realization parameters of the various kinds of lateral gratings developed during the project;
- ✓ the extensive parameter extraction for the simulation and design activities from the various realizations done by the partners
- ✓ the development (done by ORC-TTY) of numerical programs for analyzing the effect of end facets and optimizing the yield of single-mode devices with required laser characteristics
- ✓ the development (done by ORC-TTY) of a modified rate equation model, which includes the photon-photon resonance (PPR) and defines the basic criteria needed for the exploitation of the PPR in the modulation response;
- ✓ the development of procedures to analyze and design three different kinds on laser cavities adapted to exploit the PPR to extend the small signal modulation bandwidth (done by TTY-ORC and PT for different types of cavities) and the large-signal bit rate (done by PT);
- ✓ the analysis of the stability of the PPR operation in multi-section lasers and the design of various high-speed multi-section devices exploiting the PPR (done by ORC-TTY and PT for different multi-section structures);
- ✓ the development for the first time (by TN) of numerical programs for the accurate static and dynamic simulation of QD laser considering the spatial resolution in depth of the QD active region; the programs allow the analysis of structures with typical QD injection from the SCH and also the analysis of structures employing tunnel injection into the QDs;

✓ the development for the first time (by PT) of a quite general Finite Difference Traveling Wave program that can be used for the analysis and design of QD lasers and amplifiers taking accurately into account the longitudinal effects in the cavity.

The results of the modeling, simulation and design of LC-RWG gratings and of various types of lasers exploiting the PPR (CCIG, multi-section DFB and DBR lasers) as well as of QD lasers with large modulation bandwidths have been communicated / published in major conferences and scientific journals (listed in the publications tables). Excerpts from the most relevant simulation results confirmed by experiments are presented in the following paragraphs.

2.2.1. Modeling, simulation and design of the LC-RWG gratings

Regarding the methods for evaluating the LC-RWG grating coupling coefficient it was found, early in the project, that, due to different interaction with and influence on the transverse optical field distribution, the conventional methods and approximations used for evaluating the coupling coefficient of buried gratings are not accurate for LC-RWG surface gratings. The standard grating coupling coefficient formula:

$$\kappa = \frac{k_0}{2n_{eff}} \cdot (n_2^2 - n_1^2) \cdot \Gamma_g \cdot \frac{\sin(\pi m \gamma)}{\pi m} \approx k_0 \cdot (n_2 - n_1) \cdot \Gamma_g \cdot \frac{\sin(\pi m \gamma)}{\pi m} , \qquad (2.2.1\text{-}1)$$

where $k_0 = 2\pi/\lambda_0$, n_1 and n_2 are the refractive index values in the low- and high-index grating areas, Γ_g is the optical confinement factor in the grating area, m is the grating order and γ is the grating filling factor (defined as the ratio of the high refractive index grating slice length over the grating period), is relatively accurate for a small optical contrast (n_2-n_1) and large optical confinement factor in the grating and uses the approximation that $n_1+n_2 \approx 2 \cdot n_{eff}$, which is not valid for surface gratings. Our better, more accurate way to calculate the LC-RWG surface grating coupling coefficient has been presented in [3, Table 5.1]. The left panel of Fig. 2.2.1-1 shows a comparison between the LC-RWG grating coupling coefficient calculated with the standard formula (which is also used by commercial software programs like PICS3D from CrossLight Software Inc.) and with our adjusted formula and convolution approach [3, Table 5.1]. Our adjusted formula and convolution approach for calculating the LC-RWG grating coupling coefficient has been repeatedly certified by scanning electron microscopy (SEM) determination of the fabricated structures' dimensions and by experimental evaluations of the coupling coefficient through fitting measured and simulated sub-threshold emission spectra (example given in the right panel of Fig. 2.2.1-1). The figure also illustrates that by applying our improved coupling coefficient calculation procedure inconsistently or incompletely (e.g. by combining the adjusted formula with the conventional way of calculating the effective refractive index values for the grating slices) one can also get substantially incorrect coupling coefficient values.
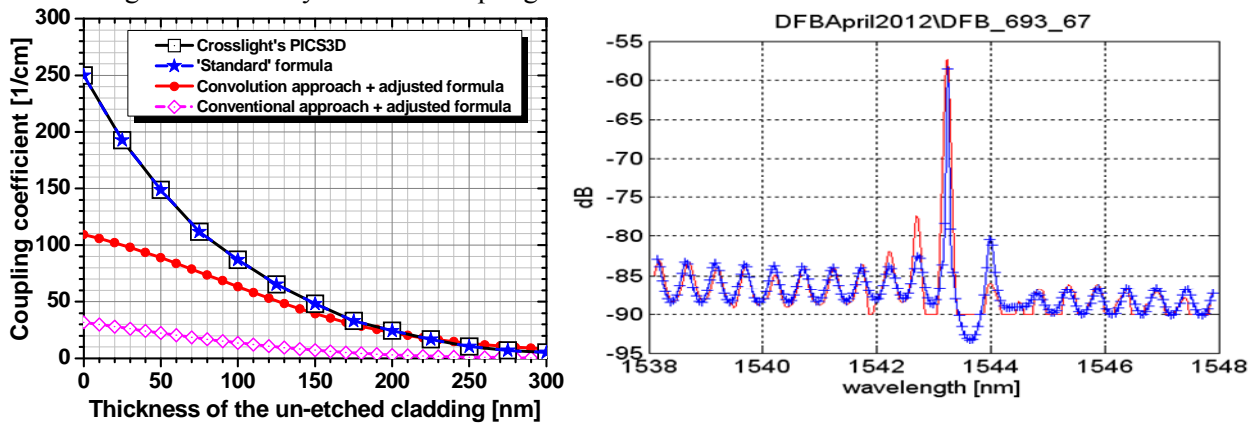

Fig. 2.2.1-1: (Left panel) LC-RWG grating coupling coefficient values calculated with the standard formula (stars), with the adjusted formula and conventional method (diamonds), with the adjusted formula and convolution method (circles) and obtained with PICS3D (squares); (right panel) coupling coefficient extraction by fitting simulated and experimental sub-threshold spectra.

The development of the programs for coupling coefficient evaluation and grating structure analysis was particularly intense in the first project period, during which ORC-TTY completed the development of its code based on finite difference, while PT completed a code based on finite element method. The coupling coefficient evaluation methods were both successfully compared with test cases, experimental results and against each-other (as illustrated in Fig. 2.2.1-2).
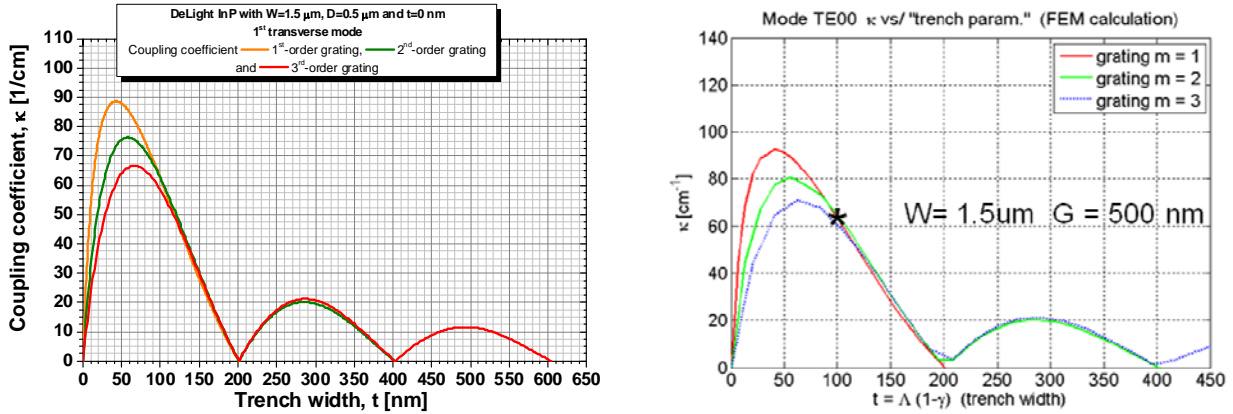
Fig. 2.2.1-2: Comparison of the 1st transverse mode coupling coefficient variation with trench width for 1st-, 2nd- and 3rd-order LC-RWG gratings (with W=1.5µm, D=0.5µm and t=0 nm), calculated with ORC-TTY's 2D Finite-Difference program (left panel) and with PT's 2D Finite-Element Method software (the differences are derived from different discretization meshes).

To illustrate the particular interaction of the LC-RWG gratings with the optical field, the upper left panel of Fig. 2.2.1-3 shows the transverse optical field distribution in a ridge-waveguide (RWG) DFB laser with buried grating while the upper-right panel of Fig. 2.2.1-3 gives, for comparison, the transverse optical field distribution in a DFB laser with LC-RWG surface gratings. The lower panels of Fig. 2.2.1-3 show the grating coupling coefficient variation with the grating filling factor calculated for 1st, 2nd and 3rd-order gratings of the corresponding structures. In the case of the buried gratings, the coupling coefficient variation with the filling factor is mainly derived from the variation of the term *sin(πmγ)* from formula (2.2.1-1), whereas the effective refractive index n_{eff} and the grating confinement factor Γ_g have only a limited variation with the filling factor. This is due to the fact that the transverse optical filed distribution does not change substantially with the grating filling factor. This is no longer valid in the case of the LC-RWG surface gratings, as can be inferred from the asymmetry in the LC-RWG grating coupling coefficient variation shown in the lower-right panel of Fig. 2.2.1-3. In the case of LC-RWG gratings the filling factor increase reduces the optical contrast between the semiconductor and grating area, thus not only increasing the effective refractive index n_{eff} but also substantially increasing the optical confinement factor in the grating area Γ_g. Consequently, much higher coupling coefficients can be obtained for LC-RWG gratings with high filling factors.
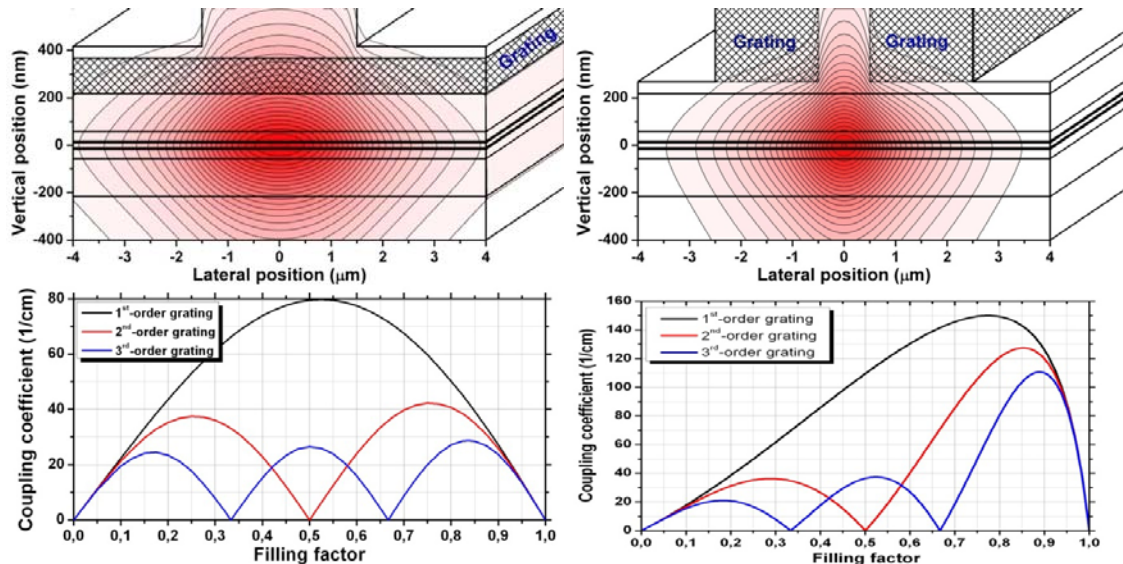

Fig. 2.2.1-3: Transverse optical field distribution in a RWG DFB laser with a buried grating (upper-left panel) and corresponding coupling coefficient variation with grating filling factor for 1st, 2nd and 3rd order buried gratings (lower-left panel) , compared with the transverse optical field distribution in a DFB laser with a LC-RWG grating (upper-right panel) and corresponding coupling coefficient variation with grating filling factor for 1st, 2nd and 3rd order LC-RWG gratings (lower-right panel).

Fig. 2.2.1-4 illustrates, besides the strong dependence of the coupling coefficient on the filling factor, the important fact that the grating trench width is a critical technological parameter for achieving a high coupling coefficient. The right panel of Fig. 2.2.1-4 shows that, until the LC-RWG grating trench width becomes very small, the coupling coefficient is similar for all grating orders if the trench width is the same.
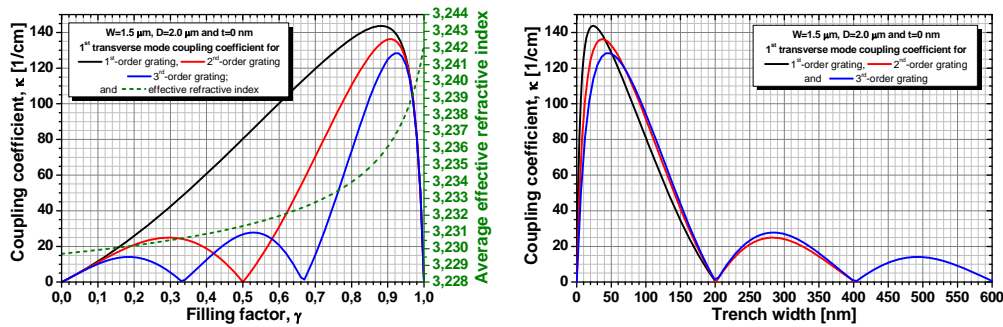
Fig. 2.2.1-4: 1st transverse mode coupling coefficient variation with grating filling factor (left panel) and, correspondingly, with grating trench width (right panel) for 1st-, 2nd- and 3rd-order gratings in a LC-RWG grating having W=1.5 μm, D=2.0 μm and t=0 nm.

The results of scanning electron microscopy (SEM) were employed in the numerically analyzed structures and used to estimate the degradation of the coupling coefficient due to imperfect realizations. In the early stages of the project we found out that, besides grating target/nominal parameters, the effective etching profiles have a substantial influence on the grating coupling coefficient. A SEM view of an imperfect grating etching profile obtained in the early experiments is given in the left panel of Fig. 2.2.1-5. The middle panel shows the calculated transverse optical field distribution in a LC-RWG grating with simulated imperfect etching profile, illustrating that the imperfect etching affects the grating profile exactly in the regions where the optical field coupling with the grating should be the strongest. The right panel of Fig. 2.2.1-5 gives the calculated reduction in the coupling coefficient, which is even more drastic for gratings with small lateral extension, D.
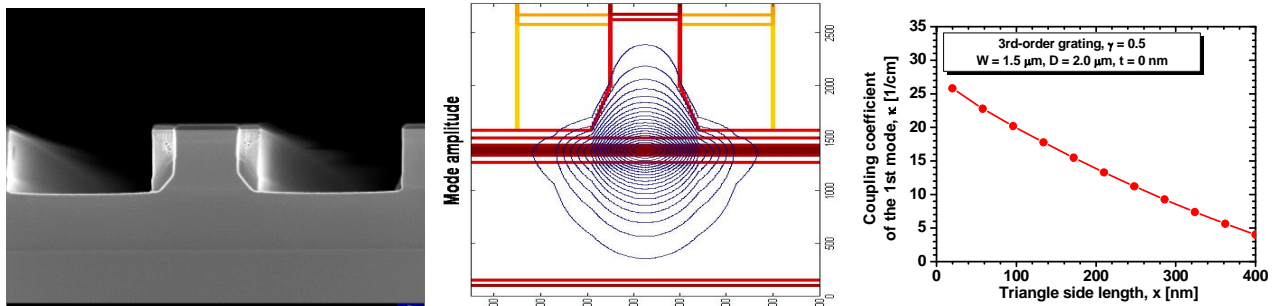

Fig. 2.2.1-5: SEM view of an imperfect LC-RWG grating profile obtained one of the first fabrication runs (left panel), calculated transverse optical field distribution in a LC-RWG grating with simulated 'imperfect' etching profile (middle panel) and variation of the coupling coefficient with increasing grating profile 'imperfection' (right panel)

Due to the relative novelty of the LC-RWG gratings their development and the corresponding analysis and simulation effort was continued throughout the project. Fig. 2.2.1-6 shows an example of the analysis done by PT of a recent LC-RWG realization by UKAS. This LC-RWG gating was intended for long grating sections with relatively small coupling coefficients.
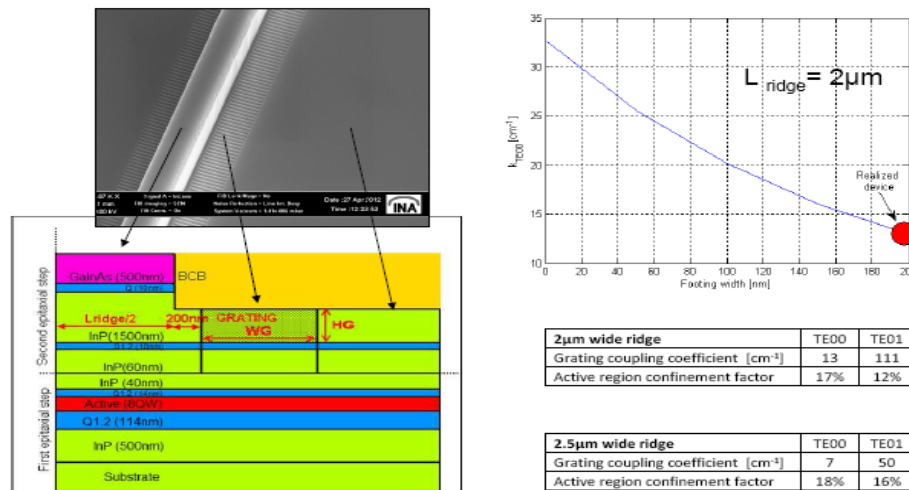

2μm wide ridge	TE00	TE01
Grating coupling coefficient [cm⁻¹]	13	111
Active region confinement factor	17%	12%

2.5μm wide ridge	TE00	TE01
Grating coupling coefficient [cm⁻¹]	7	50
Active region confinement factor	18%	16%

Fig. 2.2.1-6: PT analysis of a recent LC-RWG grating realization by UKAS: (upper part) SEM figure and coupling coefficient evaluated as a function of the footing width, (lower part) sketch of the structure and results tables.

PUBLIC

11

Conclusions for the LC-RWG grating modeling, simulation and design

- adjusted calculation procedures and formulas should be employed in the simulation of LC-RWG gratings as their particular interaction with the optical field yields most of the conventional calculation formulas (used for standard buried gratings) inaccurate;
- many of the possibilities to increase the LC-RWG grating coupling coefficient are limited (mostly by adverse effects on the other laser parameters):
  - o altering an already optimized epilayer structure in order to increase the LC-RWG grating coupling coefficient (e.g. by increasing the optical field extension into the cladding) affects the active region confinement factor (thus increasing threshold current, reducing the efficiency and differential gain, thus affecting both static and dynamic laser characteristics);
  - o increasing κ by reducing the width of the un-etched central section of the ridge (W) is limited by the detrimental effects on the electrical properties of the laser (mainly serial and differential resistance increase and heating effects);
  - o increasing κ by increasing the lateral extension of the gratings (D) has asymptotically limited effects and leads to reduced efficiency by lateral current spreading;
  - o increasing κ by increasing the etching depth beyond reducing the un-etched cladding thickness (t) to zero is limited in most cases by substantial increase in the losses;
- using narrow grating trenches (high grating filling factors) and achieving an accurate etching profile are the most effective ways to increase the LC-RWG grating coupling coefficient:
- relative high coupling coefficients can be obtained with LC-RWG gratings, even when using legacy epilayers intended for the fabrication of Fabry-Perot lasers.

It should, however, be underlined that the LC-RWG grating structure parameters (like the etching depth or, more correctly, the remaining thickness of the un-etched material from the grating to the underlying waveguide and active region, the width of the un-etched central ridge W, the lateral extension of the grating D, the filling factor γ, etc.) have a substantial influence not only on the grating coupling coefficient but also on the transverse mode discrimination. Consequently, in the case of LC-RWG surface gratings, a special care must be taken to maintain the single transverse mode operation while attempting coupling coefficient optimization by changing the grating parameters.

2.2.2. Modeling, simulation and development of the epilayer structures

The main objectives of this activity were to develop epilayer structures both having intrinsic high-speed modulation capabilities and enabling the effective use of LC-RWG surface gratings. Existing legacy epilayer structures (intended for high-speed Fabry-Perot lasers) were also investigated, mainly for evaluating their suitability for fabricating LC-RWG gratings. Also specifically-designed epilayers have been designed and studied for both 1.3 and 1.55 µm wavelength ranges. These specially-designed epilayers included 1.3 µm dilute-nitride (GaInAsN) quantum well (QW) lasers and 1.3 and 1.55 µm lasers with quantum dash (QDash) and quantum dot (QD) active regions. Tunnel-injection structures were investigated for increasing the modulation speed of QD lasers.

The most important conclusions from the effort to study and develop the epilayer structures, which have already been mentioned in the previous section, are:

- altering an already optimized epilayer structure in order to increase the LC-RWG grating coupling coefficient (e.g. by increasing the optical field extension into the cladding) affects the active region confinement factor (thus increasing threshold current, reducing the efficiency and differential gain, thus affecting both static and dynamic laser characteristics);
- most of the well-designed legacy epilayer structures (intended for high-speed Fabry-Perot lasers) can be successfully used for fabricating high-speed lasers with LC-RWG gratings.

2.2.3. Modeling, simulation and analysis of the end-facet effects

The phase of the cleaved end facet mirrors is incontrollable with respect to the grating because the cleaving cannot be accurately positioned with respect to the grating. This has effects on the side-mode-suppression-ratio (SMSR) of the modes favoured by the gratings in a DFB laser (as illustrated in Fig. 2.2.3-1) and is sometimes more critical in multi-section/multi-cavity devices.
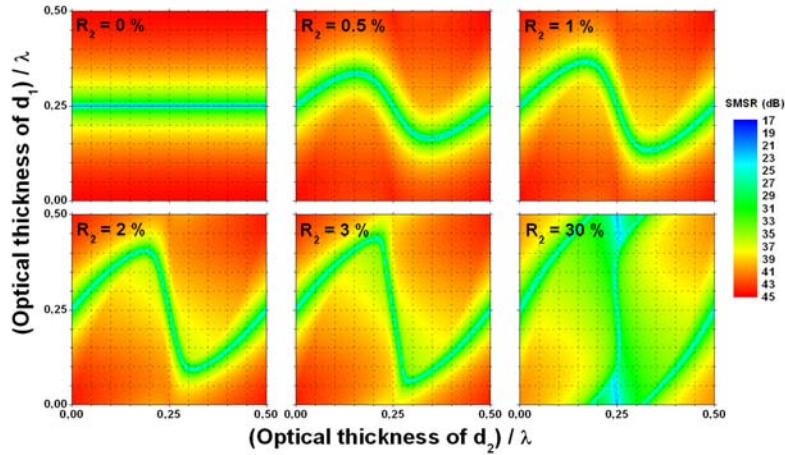
Fig. 2.2.3-1: Simulated SMSR as a function of end facet positions (d_1 and d_2) when $R_1 = 95$ % and $R_2 = 0$% to 30 %.

Furthermore, the phase of the end facet reflections has contradictory effects on the laser characteristics (as illustrated in Fig. 2.2.3-2), which leads to further reduction in the fabrication yield, taken as the proportion of devices that achieve all the target characteristics. Like the SMSR variations, I_{th}, P and $f_{3\,dB}$ variations with end facet reflection phases depend very much on facet reflectivities. Good anti-reflection coating mitigates the adverse effects of end-facet reflection mismatch, while the difference between the maximum and the minimum obtainable values for these characteristics increases and thee yield decreases when facet reflectivities increase.
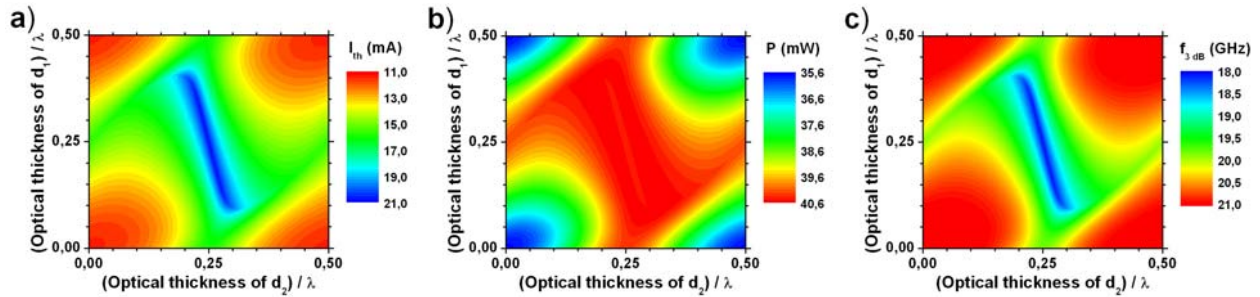

Fig. 2.2.3-2: (a) Threshold current, (b) output power at $I = 100$ mA and (c) modulation bandwidth at $I = 100$ mA when the facet positions of a 1310 nm LC-DFB structure are varied.

Conclusion of the analysis of end-facet effects

Our simulation studies have indicated that the use of at least one etched end facet, in phase with the LC-RWG gratings, especially if the etched facet has a good reflectivity (e.g. by high-reflection coating), has substantial beneficial effects both on the fabrication yield and on the stability and controllability of the photon-photon resonance in multi-section lasers. In line with this conclusion process developments have been achieved within the project, enabling the fabrication of etched end facets that can be placed with 10 nm accuracy.

## 2.2.4. Modeling, simulation and analysis of the photon-photon resonance

The development of models and the static and dynamic simulation studies towards developing devices with photon-photon resonance (PPR) were performed following two main directions. The first direction, which was mainly pursued by PT, was to develop and simplify the coupled-cavity injection grating (CCIG) laser design, whose 'standard' cavity structure comprises an active section, a grating section and a passive feedback section. The targeted simplification for the CCIG lasers was to reduce the number of sections and/or to reduce/simplify the bias (number of contacts), aiming at a stable and predictable PPR. The second direction, which was mainly pursued by TTY-ORC, was to exploit dual-mode emission lasers to achieve stable, controllable and predictable PPR.

Regarding the development of the CCIG design, PT has developed a set of guidelines for the design of CCIG structures, which were capable of large-signal modulation up to 40Gbit/s in simulation tests [21, Table 5.1]. However, it was found that, due to the high sensitivity to the cavity parameters, a very good control of these cavity parameters is necessary during the fabrication process in order to achieve an extended modulation

bandwidth. This high sensitivity led to unsuccessful realizations based on CCIG cavities. Consequently, the efforts to develop the CCIG design at PT turned later on using a DBR cavity with AR-coated facet at the grating side, to which the design guidelines developed by PT for CCIG lasers were applied successfully. During the investigation of these DBR-based cavities, in the last part of the project, a better design procedure was found, allowing a precise positioning of the PPR at the frequency of interest. With this more precise design procedure there were designed DBR-based cavities with PPR at 25, 35 and 45 GHz that theoretically allowed obtaining large signal modulation transmission well above what was targeted by this project. A first realization of these structures allowed showing for the first time a PPR effect in a DBR laser, but the large signal transmission at high bit rate was not yet achieved. Fig. 2.2.4-1 shows recent results obtained by PT regarding the extended modulation bandwidth in DBR lasers exploiting PPR.
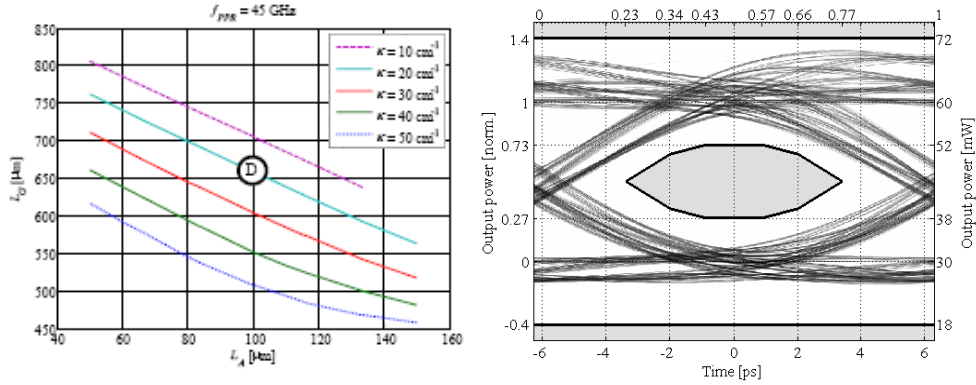
Fig. 2.2.4-1: DBR laser cavity design map for PPR at 45GHz (left) and eye diagram (right) for a NRZ PRBS bit pattern at 80Gbit/s.

The left panel of Fig. 2.2.4-1 gives the calculated active section and grating section lengths required to achieve PPR at 45 GHz for different grating coupling coefficients, according to the guidelines developed by PT. The chosen operating point, with a small value of the coupling coefficient, is well compatible with the LC-RWG gratings fabricated in the project. The right panel of Fig. 2.2.4-1 shows the eye diagram at 80 Gbit/s obtained under a proper operation condition of the lasing mode, achieved by grating current tuning [29, Table 5.1].

In order to study the possibility to extend the direct modulation bandwidth in dual-mode lasers ORC-TTY has developed a modified rate-equation model that takes the PPR into account by treating the longitudinal confinement factor as a dynamic variable [23, Table 5.1]. The differential rate equations including the extra term resulted from taking the quantum well confinement factor as a dynamic variable are the following:

$$\frac{d}{dt}\begin{bmatrix} dN \\ dN_P \end{bmatrix} = \begin{bmatrix} -\gamma_{NN} & -\gamma_{NP} \\ \gamma_{PN} & -\gamma_{PP} \end{bmatrix}\begin{bmatrix} dN \\ dN_P \end{bmatrix} + \begin{bmatrix} \dfrac{\eta_i}{qV}dI \\ (N_p v_g g + R'_{sp})d\Gamma \end{bmatrix} \tag{2.2.4-1}$$

where γ_{NN}, γ_{NP}, γ_{PN} and γ_{PP} are rate coefficients, as defined in [1]. By following the same analysis of the small-signal response to modulation as in [1], the small-signal photon density, including the influence of the extra term, results as:

$$N_{p1} = \frac{\eta_i I_1}{qV} \cdot \frac{\gamma_{PN}}{\Delta} + (N_p v_g g + R'_{sp}) \cdot \frac{(\gamma_{NN} + j\omega)}{\Delta} \cdot \frac{d\Gamma}{e^{j\omega t}} \tag{2.2.4-2}$$

where $\Delta = (\gamma_{NN} + j\omega) - (\gamma_{PP} + j\omega) + \gamma_{NP}\gamma_{PN}$.

The modulation transfer function including the influence of the extra term resulted from the (space and) time variation of the confinement factor, can be written as:

$$H(\omega) = \frac{\eta_i}{qV} \cdot \frac{\displaystyle\int_0^T \frac{\gamma_{PN}}{\Delta}dt}{T} + \frac{1}{I_1 \cdot T} \cdot \int_0^T \frac{(\gamma_{NN} + j\omega) \cdot (N_p v_g g + R'_{sp})}{\Delta \cdot e^{j\omega t}} \cdot \frac{d\Gamma}{dt}dt \tag{2.2.4-3}$$

where T is the time interval for which the phase difference between the dominant longitudinal modes is maintained. The first term in (2.2.3-3) resembles the traditional modulation transfer function, with γ_{PN} and Δ

---

[1] L. A. Coldren and S. W. Corzine, *Diode lasers and photonic integrated circuits,* John Wiley & Sons, New York (1995).

taken as time-dependent, while the second term is resulted from considering the (space and) time dependence of the confinement factor. This second term introduces the supplementary PPR peak placed at a frequency equal with the frequency difference between the two dominant longitudinal modes. The model indicates that a primary condition for achieving the PPR is to have the dominant modes phase-locked for long enough (quasi-phase-locked). Therefore, besides the large frequency difference between modes, the main reason for not achieving a significant PPR peak in conventional multimode lasers is that they do not provide a mechanism to maintain the phase difference between modes for long enough.

The difficulty in extending the direct modulation bandwidth of the lasers is not related to placing the PPR at high frequencies but to achieving a flat modulation bandwidth between the carrier-photon resonance (CPR) and PPR. We have managed to design and fabricate multi-section DFB lasers with LC-RWG gratings having quasi-phase-locked longitudinal modes with frequency differences ranging from 14 GHz to 1.3 THz. Fig. 2.2.4-2a and 2.2.4-2b show measured and simulated dual-mode emission spectra with a frequency separation of 47 GHz and 1 THz, respectively. The (relative) intensity noise measurements for the dual-mode lasers confirm that the modes are indeed quasi-phase-locked. Fig. 2.2.4-2c shows the intensity noise (IN) spectrum (not normalized to the optical power of the laser) obtained from a 1.6 mm long multi-section laser emitting at 1.55 μm and designed for dual-mode emission with 20 GHz frequency separation. The laser was among those exhibiting a multimodal emission (with several longitudinal modes lasing, as can be observed in the inset, due to the un-optimized LC-RWG grating geometry, which led to a relatively small coupling coefficient). A clear and sharp PPR peak in the laser IN spectrum indicates that, from the multiple longitudinal modes, only the grating-favoured modes, spaced at 20 GHz are indeed quasi-phase-locked. The difference between the CPR and PPR IN features is clearly observable.
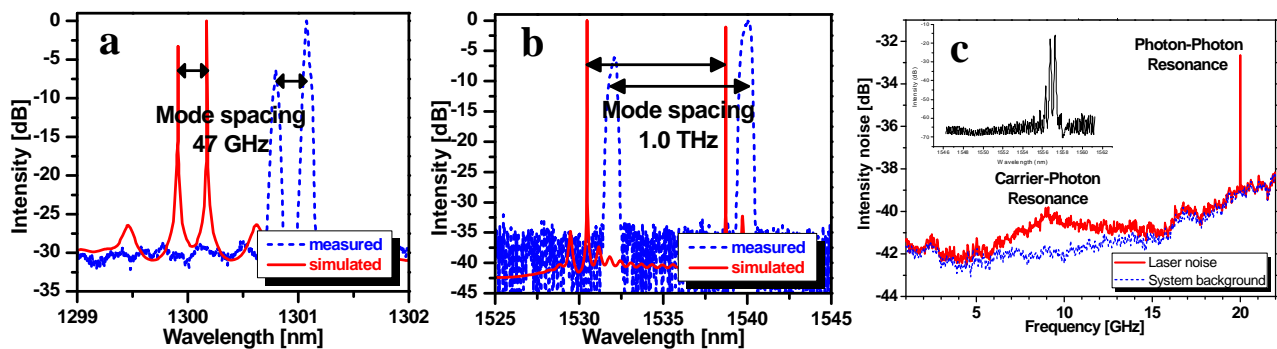
Fig. 2.2.4-2: Simulated and measured dual-mode emission spectra with quasi-phase-locked longitudinal modes having (a) 47 GHz and (b) 1.0 THz frequency spacing and (c) intensity noise spectra measured for a 1.55 μm multi-section LC-RWG grating laser emitting multiple longitudinal modes.

The difficulty of obtaining a relatively flat/smooth modulation response between the CPR and the PPR is illustrated in Fig. 2.2.4-3a, which shows the simulated small-signal modulation responses for a laser with PPR at 47 GHz, calculated for different side-mode-suppression ratios (SMSRs) between the two quasi-phase-locked modes, varying between 0 (power equally distributed between the two modes) and 60 dB. As can be seen, if the PPR is far away from the CPR, there is a substantial gap in the modulation response between the two resonances. Filling this gap is essential for extending the direct modulation bandwidth.
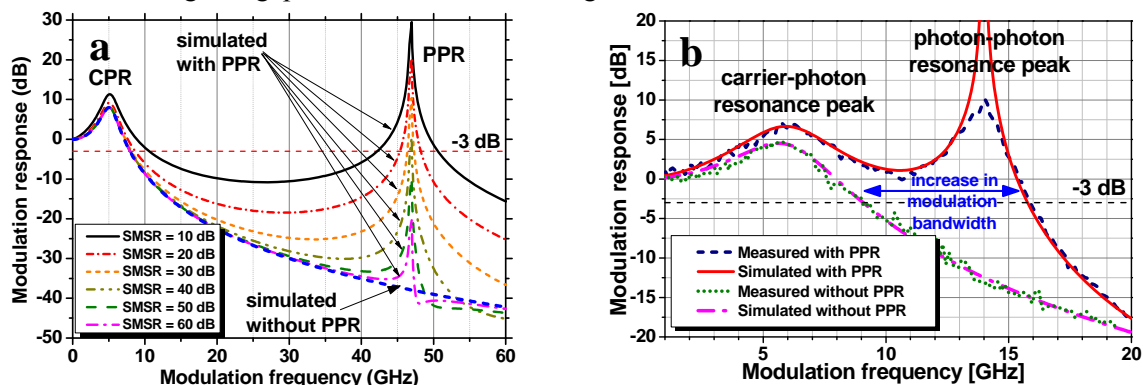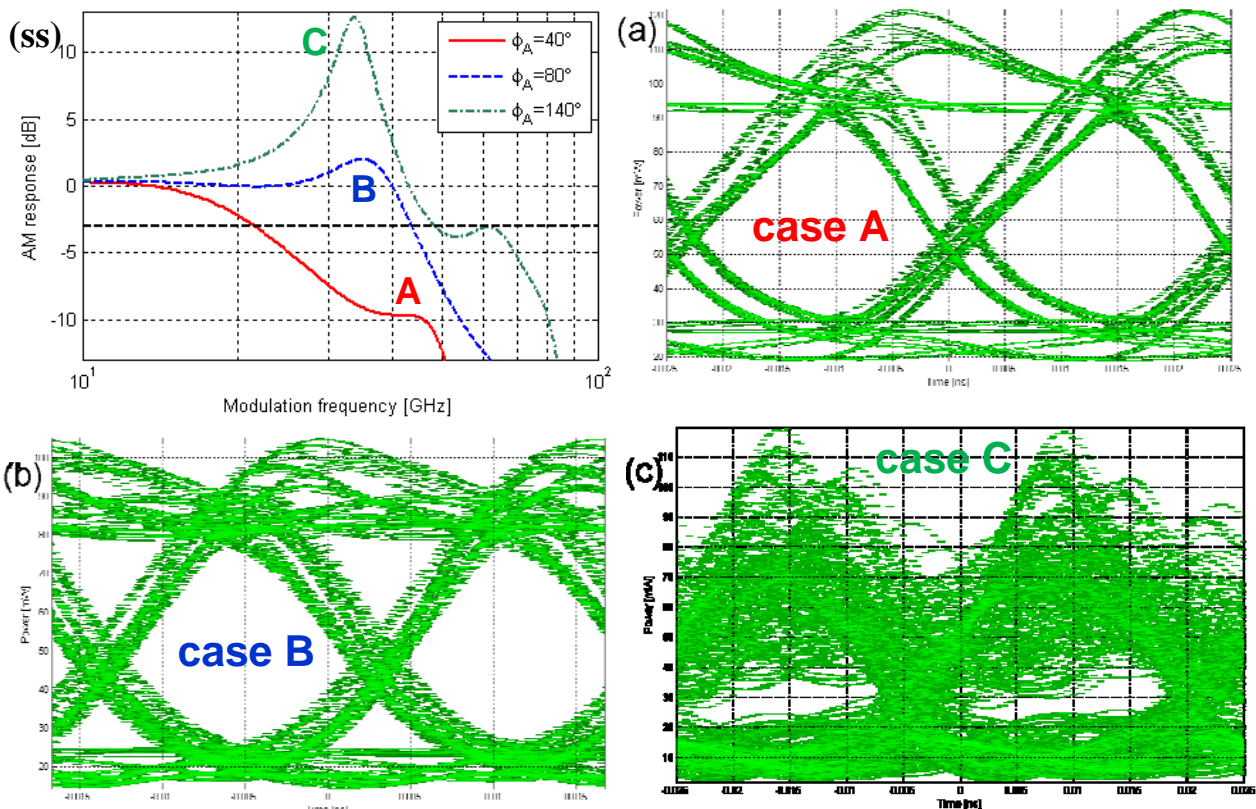
Fig. 2.2.4-3: (a) Simulated small-signal modulation response of a multi-section DFB laser with LC-RWG gratings, having variable mode-suppression ratios between the two grating modes and (b) measured and simulated small-signal modulation responses for two types of lasers, one without PPR and the other with PPR at 14 GHz.

The experiments have confirmed that the dual-mode frequency spacing and, consequently, the PPR frequency can be largely determined by the longitudinal structure of the multi-section DFB/DBR lasers. However, the experiments have also shown that the modulation responses of the dual-mode lasers with large frequency differences between the quasi-phase-locked modes are hampered by the large and deep dip between the CPR and the PPR. Therefore, due to the difficulty in achieving a relatively flat modulation response with PPR at higher frequencies, the project has first targeted the fabrication of lasers with PPR frequencies below and around 20 GHz. Fig. 2.2.4-3b illustrates the accuracy of PPR modelling as well as the achievable increase in small-signal modulation response obtained by exploiting the PPR. It shows measured and simulated direct modulation responses for two types of DFB lasers fabricated in the same fabrication run and from the same legacy epiwafer (with the epilayer structure intended for the fabrication of Fabry-Perot lasers at 1.55 μm). The first laser type was a single-mode single-longitudinal-section DFB laser with LC-RWG gratings, which does not exhibit PPR. The second type was a much longer multiple-longitudinal-section DFB laser with similar LC-RWG gratings but having a longitudinal structure designed to induce PPR at ≈ 14 GHz. The small-signal modulation response simulation for the laser with PPR was fitted to the measurement by assuming a SMSR of 23 dB between the two quasi-phase-locked modes.

Since the -3 dB small-signal modulation bandwidth may not be indicative of the large-signal modulation capability, particularly in case of a small-signal modulation response with substantial variations across the bandwidth, we have also analyzed the small-signal modulation response and the corresponding large-signal modulation capability using a Finite-Difference Travelling-Wave program developed by PT [20, Table 5.1].

Fig. 2.2.4-4: (ss) Simulated small-signal modulation response for different phases of the cleaved facet mirror reflectivity in a multi-section laser with high-frequency PPR; (a) 40Gbit/s eye diagram computed for case A, having an extinction ratio (ER) = 6dB; (b) 60Gbit/s eye diagram computed for case B, having ER = 4.5dB; (c) 40Gbit/s eye diagram computed for case C.

Fig. 2.2.4-4ss shows the small-signal modulation response simulated for three different phases of the cleaved-facet mirror reflectivity in a multi-section laser (a similar result can be obtained by changing the bias current in one of the laser sections). Large-signal eye diagrams were calculated for the three values of cleaved-facet reflectivity phase, using a non-return-to-zero pseudorandom bit sequence signal at different modulation bit rates. The cases were chosen to compare the situation when the PPR peak is small, under the -3 dB level and with minimal influence on the -3 dB small-signal modulation bandwidth (case A); the situation when the PPR peak is moderate and the small-signal modulation response is extended in a relatively flat way (case B); and the situation when the PPR peak is very pronounced (case C).

In case B, as expected, an eye diagram with a reasonably good extinction ratio (ER = 4.5 dB) could be obtained beyond the -3 dB small-signal modulation bandwidth, at 60 Gbit/s. The simulations also confirm that a strong PPR peak (case C) is dramatically reducing the eye opening even at 40 Gbit/s, although the large-signal modulation responses shouldhave been good at this bit rate if the small-signal modulation response would be flat. Surprisingly, a good 40 Gbit/s large-signal modulation response, beyond the –3 dB small-signal modulation bandwidth, could be obtained in case A, when the PPR peak is well below the -3 dB level and does not influence substantialy the small-signal modulation bandwidth. This indicates a significantly broader operational range where the large-signal modulation capability can be extended by exploiting the PPR. Unfortunately,these simulation results were obtained towards the end of the project, in search of the causes for the poorer-than-expected large-signal modulation responses, and could not be applied within the project.

2.2.5. Static and dynamic modelling and simulation

Regarding the static and dynamic modeling and simulation for DFB/DBR edge-emitting lasers (EELs) the effort was aimed to give input to the DFB/DBR laser development and fabrication (at TTY-ORC, UKAS, UWUERZ and III-V Lab) but also to enable parameter extraction from the static and dynamic characterization of the fabricated lasers. It should be mentioned that, following the parameter extraction, a good agreement was found between measurements and simulations [16, Table 5.1].

Besides the static and dynamic modelling, simulation and analysis already mentioned in the previous sections, TN developed an advanced spatially resolved model for QD lasers, the first of this kind for laser structures with QD active regions [32, Table 5.1]. Since the main characteristic targeted by the project is an increased direct modulation bandwidth, the QD laser model developed by TN has also the capability to analyze QD heterostructures with tunnel injection. The model was applied to improve the dynamic characteristics of the QD lasers fabricated by UKAS. Fig. 2.2.5-1 illustrates the improved dynamic characteristics obtained using this model, which were confirmed by small-signal and large-signal modulation measurements (reported in section 2.6 and illustrated in Fig. 2.2.5-2). Also PT has developed its Finite Difference Travelling Wave (FDTW) code for QD lasers taking into account the QD inhomogeneous broadening and separate electron and hole dynamic. The FDTW code for QD active regions has been validated successfully and recent experimental data have been reported in the literature [20, Table 5.1].
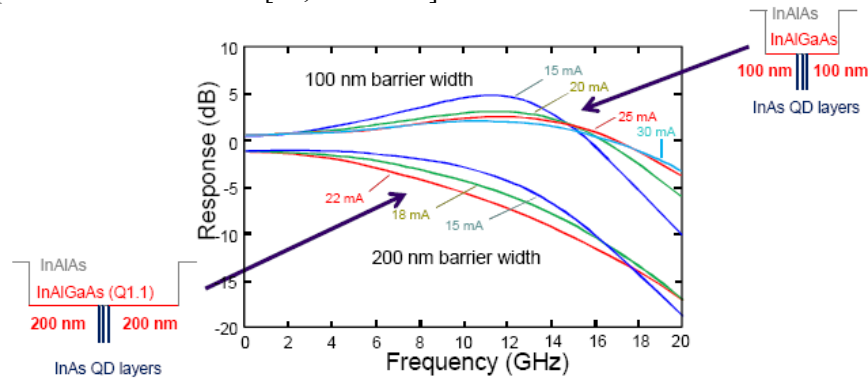

Fig. 2.2.5-1: Dynamic small-signal modulation obtained for the initial epilayer structure of the QD lasers (shown on the left) and for the improved epilayer structure (shown on the right)
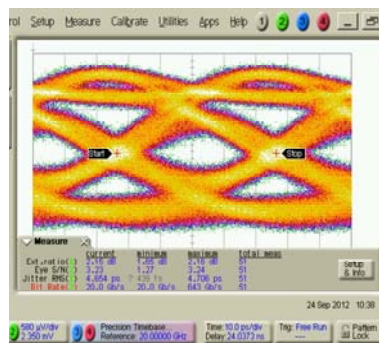

Fig. 2.2.5-2: Room-temperature measured eye diagrams at 20 Gbit/s for the QD lasers with improved epilayer structure

PUBLIC

2.3. Achievements in WP3 "Development of growth technology & epiwafer growth"

The main objective of WP3 was to provide suitable epiwafers for the fabrication of DeLight lasers. Several types of epiwafers were targeted. Legacy epiwafers operating both at 1.3 and 1.55 µm (intended for the fabrication of high-speed Fabry-Perot lasers) which have been found suitable for the fabrication of effective LC-RWG gratings, have been either provided from storage or grown without any epilayer modification. Also specifically-designed epiwafers have been grown and tested both for 1.3 and 1.55 µm wavelength ranges, targeting intrinsic high-speed modulation capability and suitability for the fabrication of LC-RWG gratings. These specially-designed epilayers included 1.3 µm dilute-nitride (GaInAsN) GaAs-based quantum well (QW) lasers and 1.3 and 1.55 µm InP-based lasers with QW, quantum dash (QDash) and quantum dot (QD) active regions. Tunnel-injection structures designed in WP2 were also experimentally investigated. The specifically-designed epilayer structures took into account the particular requirements for the fabrication of LC-RWG gratings employing nanoimprint lithography – like the use of etch-stop layers.

In terms of new epilayer structure development the most important achievements were obtained with QD lasers, which were extensively studied and optimized according to the simulations. The most advanced epilayer structure is given schematically in Fig. 2.3-1. The epilayer contains six QD layers separated by 20 nm InAlGaAs barriers and the separate-confinement / waveguide region is 100 nm wide on each side of the QD active region. This design maximizes the gain and minimizes the transport time limitation, leading to fast laser responses.
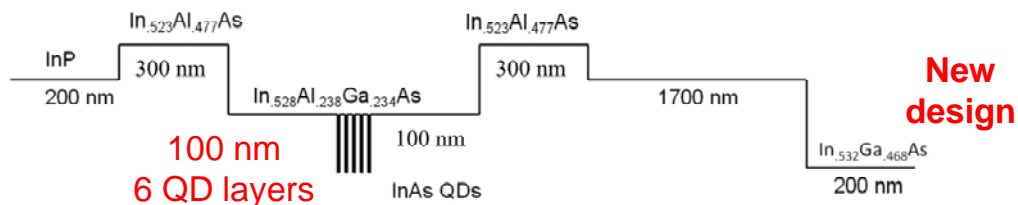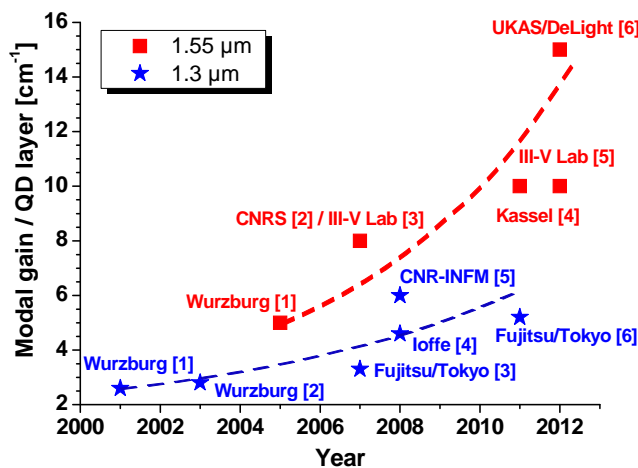

Fig. 2.3-1: Schematic of optimized QD laser structure

The optimized growth conditions of the QD active region enabled record-high modal gain values, illustrated in Fig. 2.3-2, which enabled the fabrication of short-cavity RWG QD lasers with record values in direct digital modulation (> 20 Gbit/s), as reported in section 2.6.

[1] J.P. Reithmaier et al., JPD 38, 2088 (2005)
[2] E. Homeyer et al., JAP 46, 6903 (2007)
[3] F. Lelarge et al., JSTQE 13, 111 (2007)
[4] C. Gilfert et al., APL 98, 201102 (2011)
[5] N. Chimot et al., IPRM 2012, We-1D2
[6] UKAS/DeLight (2012)

[1] F. Klopf et al., PTL 13, 764 (2001)
[2] R. Krebs et al., JCG 251, 742 (2003)
[3] M. Ishida et al., JAP 101, 013108 (2007)
[4] M.V. Maximov et al., SST 23, 105004 (2008)
[5] A. Salhi et al., NT 19, 275401 (2008)
[6] K. Takada et al., EL 47 (3) (2011)

Fig. 2.3-3: Progress in QD laser modal gain at 1.3 and 1.55 µm

Although specifically designed epilayer structures could be optimized for fabricating high-speed lasers with LC-RWG gratings it was also found that most of the well-designed legacy epilayer structures (intended for high-speed Fabry-Perot lasers) can also be successfully used for fabricating high-speed lasers with LC-RWG gratings.

2.4. Achievements in WP4 "Development of device processing technologies"

The main objectives of WP4 were:

- the development of a ultra-violet nanoimprint lithography (UV-NIL) technology capable of accurately imprinting the masks required by the device fabrication process;
- the development of UV-NIL-compatible low-damage etch processes both for GaAs- and InP-based epiwafers capable of producing LC-RWG gratings with high aspect ratio (trench width / trench depth) and good/accurate etching profiles;
- the fabrication of high-speed DFB/DBR and multi-section lasers with LC-RWG gratings;
- the development of a UV-NIL-compatible, low-cost, high-throughput / large-scale fabrication process for the high-speed lasers with LC-RWG gratings.

Following these objectives, the main scientific and technical results achieved in WP4 are:

- ✓ a UV-NIL process was developed, which enables the imprinting of process masks for the fabrication of LC-RWG gratings down to 1st order with high throughput;
- ✓ UV-NIL-compatible, LC-RWG grating fabrication processes were successfully developed for GaAs-based (at 1.3 µm) and InP-based (at 1.3 and 1.55 µm) lasers;
- ✓ several LC-RWG grating structure geometries were tested and developed in order to achieve high-enough coupling coefficients and low losses;
- ✓ a new high-yield 1st order grating fabrication process was developed, based on epitaxial structures with two etch-stop layers;
- ✓ a new gas-chopping process was developed for InP, obtaining record high aspect ratios of more than 40 with a 100 nm trench width (a patent was applied for this process);
- ✓ a process for fabricating the LC-RWG gratings and phase-matched etched facets in the same etching step has been developed;
- ✓ InP based DFB, DBR and multi-section lasers with PPR designed for 20 – 40 GHz were successfully fabricated from different types of epiwafers (including legacy epiwafers intended for high-speed Fabry-Perot lasers) with different surface grating fabrication techniques;
- ✓ a new two-section DBR laser design was realized for the first time, with a clear PPR bandwidth enhancement;
- ✓ short-cavity RWG QD lasers with record values in direct digital modulation (> 20 Gbit/s) were fabricated for the first time.

2.4.1. Development of UV-NIL

A highly productive and cost-effective UV nanoimprint lithography (UV-NIL) technique, was developed, which can imprint a full wafer (without automation support) in a few minutes and enables pattern resolutions beyond the limitations set by the diffraction and scattering for the conventional projection techniques. The developed UV-NIL process starts with fabricating a master template imprinted by electron-beam-lithography. The master template is subsequently replicated to UV-transparent soft and flexible NIL stamps. The use of stamps to create the process masks onto the epiwafer enables multiple processes based on a single master template (which is the most time-consuming and expensive part of the UV-NIL process). This is effective not only for production but also for process development where numerous imprints of the same pattern are required for process tests.

The NIL stamps have contradictory requirements. On one hand, in order to imprint small features with high accuracy they should have a high elastic modulus and great surface hardness. On the other hand, in order to adapt and conform to a fragile substrate with surface imperfections (non-flatness, defects and hard particles that might be caught between the stamp and the substrate), the stamp has to be soft and flexible but still rigid to lateral deformations to enable the accurate reproduction of the imprint. Fig. 2.4.1-1 illustrates the advantages of using a soft stamp when surface imperfections and particles are un-avoidable.
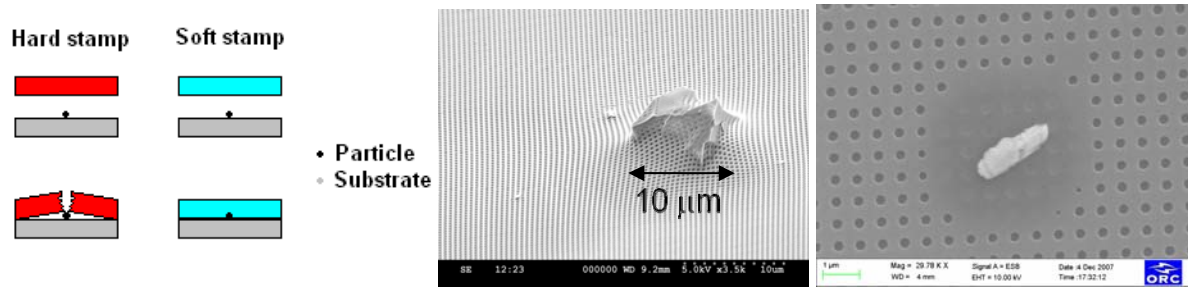
Fig. 2.4.1-1: Imprint with hard and soft stamp when a particle or a defect is caught between the stamp and the substrate (left panel).
and SEM picture examples of soft stamps' toleration to particles and defects (middle and right panels)

Our soft and flexible UV-NIL stamp structures, shown in the left panel of Fig. 2.4.1-2 were specifically developed to fulfill all the conflicting NIL stamp requirements. Beginning from the imprinting side, the fabrication of the stamps starts with a thin layer of polydimethylsiloxane (PDMS) spun on the master template. Then a thin flexible glass plate is placed onto the uncured PDMS and the ensemble is cured. After curing, the glass and hard-PDMS ensemble is separated from the master template and attached to a thick slab of soft PDMS. The use of the thin glass layer prevents the lateral stretching of the patterns while maintaining the stamp soft and flexible. If the flexibility is not critical the ensemble can be attached to a thicker glass substrate. The softness and flexibility enable the three-layer stamps to adapt to wafer-scale nonflatness (i.e. particles, curvature, waviness etc.), as illustrated by the imprint over a 10 µm particle shown in the middle panel of Fig. 2.4.1-1, making possible full-wafer imprinting with low pressure (50-500 mbar). The flexibility also eases stamp separation after imprinting (which is desired when working with fragile wafers). The UV-transparency of the stamps offers the possibility to use low viscosity UV-curable polymers. The low viscosity promotes fast process throughput and, because the resist is UV-cured, the imprint sequence does not require heating (which may cause replication inaccuracies due to different thermal expansion coefficients).
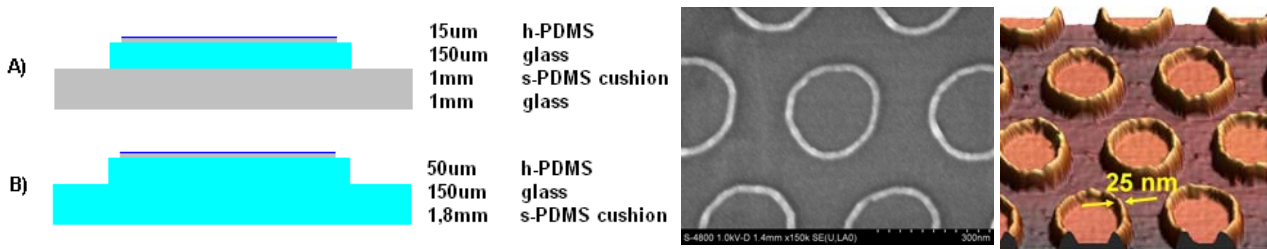
Fig. 2.4.1-2: (Left panel) UV-NIL stamp structures with (A) firm and (B) soft substrates; (middle and right panels) SEM and AFM imagers of 20-25 nm narrow-line imprints achieved with UV-NIL

Several UV-NIL stamp structures have been tested to increase the imprinting accuracy and reduce the thickness of the residual resist layer left after imprinting [1, 5, Table 5.1]. The middle and right panels of Fig. 2.4.1-2 show SEM and atomic force microscopy (AFM) images of thin 20-25 nm lines imprinted by UV-NIL. The AFM picture in the right panel of Fig. 2.4.1-2 also illustrates the problem of the residual layer left in the imprinted areas. Improved stamp geometry and a better way to apply the load to the stamp led to significant imprint profile improvements (illustrated in the left panel of Fig. 2.4.1-3) and to a substantial reduction in residual layer thickness (sub 10 nm residual layer thickness was obtained with the new mask layout). The developed UV-NIL process enabled the accurate reproduction of templates with under 100 nm feature sizes to etch masks used in the device processing (as illustrated in the right panel of Fig. 2.4.1-3).
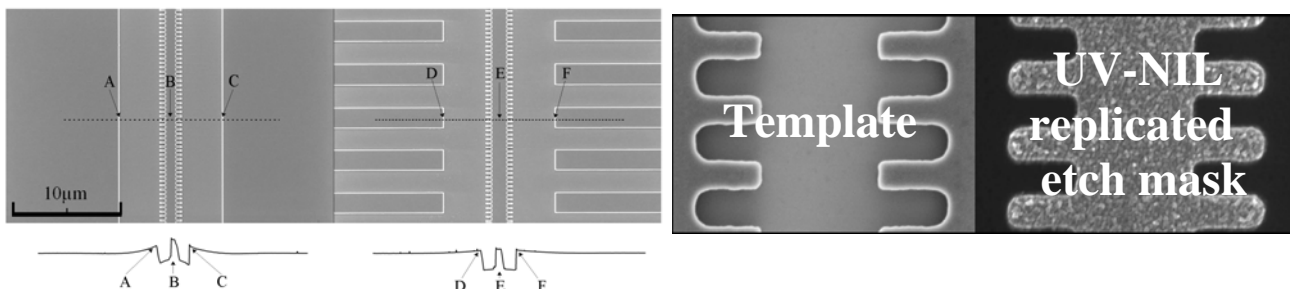

Fig. 2.4.1-3: (Left panel) Old stamp structure and imprinted profile compared with improved stamp structure and imprinted profile; (right panel) master template profile with 100 nm range features and aluminium etch mask replicated using UV-NIL

2.4.2. Development of etching and LC-RWG grating structures

Various grating structures, including shallow and deeply etched LC-RWG gratings, were developed and tested in GaAs- and InP-based material systems and for different emission wavelengths (1, 1.3 and 1,55 µm) by applying either UV-NIL or electron beam lithography (EBL). The purpose was to find out the most suitable approach in terms of cost, yield, performance, ease of processing and potential throughput. The grating definition for the devices fabricated at UKAS and UWUERZ was done with EBL, which is generally the method of choice in research and development since it offers great flexibility, very good resolution and high alignment accuracy. Furthermore, it can be used to define structures on an already patterned and therefore non-planar surface. The drawback is the serial nature of the exposure, making it inherently slow and not suitable for cheap large volume mass production. Another drawback for process development derives from the fact that the full imprinting process has to be performed for each separate process test of a given grating structure. The grating definition for the devices fabricated at ORC was done with UV-NIL, which is more cost effective (mainly due to the reduced cost of ownership for the equipment and to the higher throughput). Supplementary, both in production and in process development only the stamping is repeated, while the most costly and time-consuming steps (template and stamp fabrication) are performed only once. The NIL has, however, the disadvantage that it is applicable only to planar surfaces. Consequently, significant efforts have been made to adapt all the processes developed for the fabrication of the surface gratings so that they are fully compatible with the UV-NIL technology and can be incorporated in low-cost high-throughput production.

The simulations have indicated that a narrow grating trench width etched almost completely through the cladding layer, close to the waveguide layer, is one of the key factors for obtaining a high coupling coefficient with low losses. Consequently, the etching experiments at ORC have investigated the fabrication of LC-RWG with deep narrow trenches (i.e. having a relatively high depth/trench width aspect ratio). Fig. 2.4.2-1 shows SEM pictures of LC-RWG gratings etched ≈1.2 µm deep in GaAs/AlGaAs with a period of Λ=180nm and a variable filling factor: γ = (grating 'wing' width / grating period) = 40/180, 60/180 and 80/180 from the left to the right panel. While the gratings with a low filling factor $\gamma=\Lambda_1/\Lambda$=40/180 (in the leftmost panel) were deformed and broke during the processing, the gratings with higher filling factor γ=60/180 and γ=80/180 (in the second and third panels from left) were stable, pointing out that the technological difficulty is less in obtaining narrow trenches and more in obtaining narrow and stable grating 'wings'.
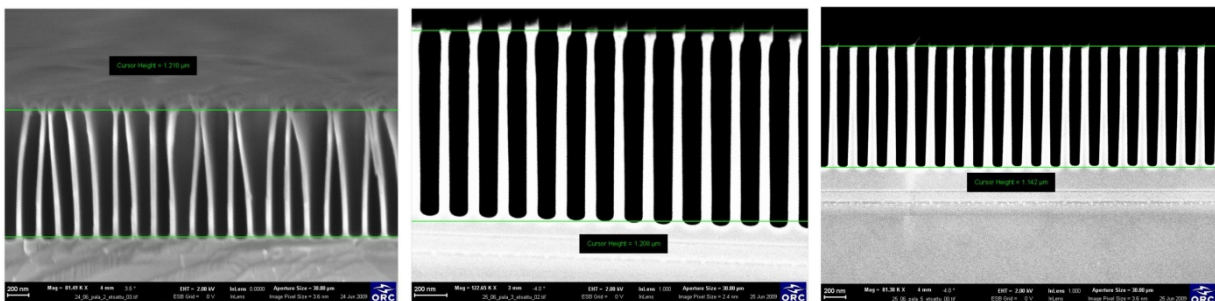
Fig. 2.4.2-1: Cross section SEM views of LC-RWG gratings with Λ=180 nm period and trench widths Λ_2 of 140, 120 and 100 nm (first, second and third panel from left, respectively)

The narrow trench experiments, which demonstrated state-of-the-art results in high-density high-aspect ratio nanopatterns, led to several conclusions regarding the fabrication of LC-RWG gratings:
- high aspect ratio gratings with grating trench widths in the range of 100 nm are technologically achievable, enabling higher coupling coefficients (as pointed out in section 2.2.1);
- a good control of the grating trench depth and width can be obtained even without etch stop layers;
- the developed procedure is suitable for mass-fabrication due to the high etch rate (> 1 µm/min) and uniformity of etched gratings across large areas.

Different geometries of the LC-RWG gratings were tested in order to achieve both a high-enough coupling coefficient and a high injection efficiency. Achieving good coupling was mainly limited by aspect-ratio-dependent-etching (ARDE), which slowed the etching in nano-size areas. This ARDE effect led to un-etched pockets at the bottom of the gratings (as can be seen for the 1st LC-RWG grating structure presented in Fig. 2.4.2-2), exactly in the areas where the optical field should couple with the gratings. Better grating profiles were obtained by adjusting the process parameters and by using a more uniform distribution of the areas to be etched (as can be seen for the 2nd LC-RWG grating structure presented in Fig. 2.4.2-2). Since a large lateral

PUBLIC

extension, *D*, of the LC-RWG gratings leads to increased lateral leakage of the pump current, an improved structure, with longitudinal current isolation trenches was also tested (the 3rd LC-RWG grating structure presented in Fig. 2.4.2-2). Unfortunately, the yield of working devices having the 3rd LC-RWG grating structure was poor. Since the low yield was mainly caused by short circuits occurring across the relatively narrow longitudinal current isolation trenches, an improved 4th LC-RWG grating structure, with wider current isolation trenches was employed in the latest device fabrication runs. This geometry yielded experimentally-evaluated coupling coefficients of ~20 cm^{-1} for 3rd-order LC-RWG gratings with ~0.5 filling factors.
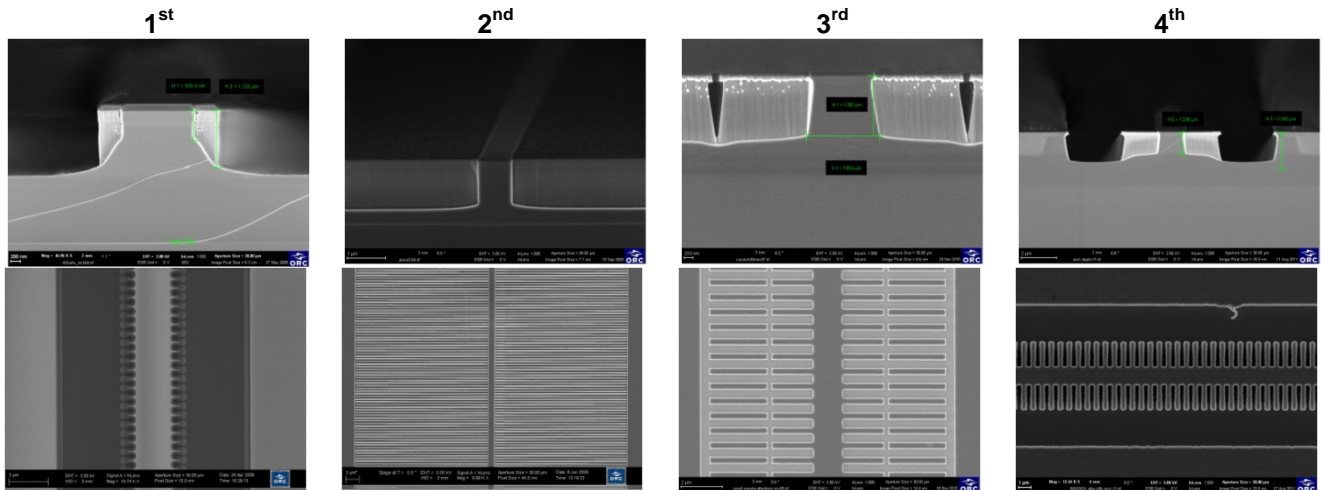
Fig. 2.4.2-2: SEM images of the main grating geometries tested at ORC. The top row gives the grating profiles seen from the facets and the bottom row gives top views of the respective grating layouts.

Several other LC-RWG surface grating structures have been investigated in the project. Due to the increased losses brought by deep etching (especially when the etching penetrates the active region) the etching depth of most LC-RWG grating structures was kept well above of the active region (usually the etching targeted the complete or almost complete removal of the top contact and cladding layers, with an important LC-RWG grating parameter being the thickness of the remaining un-etched cladding). However, surface-defined gratings deeply etched through the active region (D-SDGs) have also been tested with relative success.

Other approaches were explored in order to investigate the possibilities to avoid ARDE effects in high-aspect-ratio deeply-etched gratings. One such approach was a shallow lateral grating (SLG) structure with a non-planar grating fabrication process, which was developed at UKAS based on a new epitaxy from Alcatel-Thales III-V Lab. The new epitaxy has two additional etch stop layers only 100 nm apart, just above the active region and allows the accurate definition of 1st-order shallow lateral grating geometries with relatively large coupling coefficients and limited lateral current leakage.
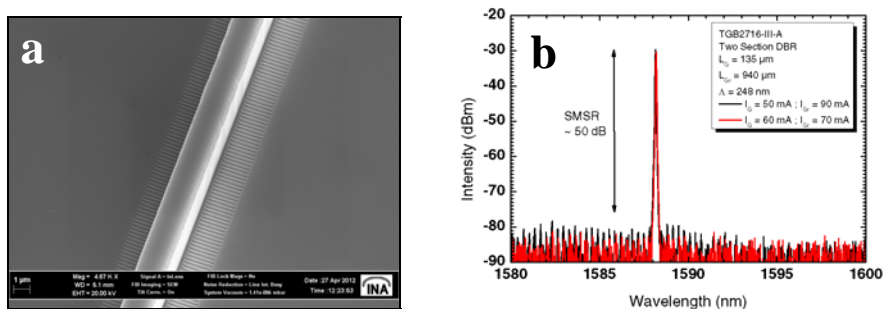
Fig. 2.4.2-3: (a) SEM image of a fully processed 1st order shallow lateral grating before planarization and metallization; (b) emission spectra of a DBR laser with 1st order shallow lateral gratings showing 50 dB SMSR at different operation conditions.

Fig. 2.4.2-3a shows a SEM picture of a DFB laser with such SLGs after the grating etch and mask removal. Due to the well controlled geometry and shallow etch step, the fabrication process was very reproducible and exhibited a very high yield (> 90% of single mode devices) even for the realization of 1st order gratings. Fig. 2.4.2-3b shows a stable single mode spectrum with ≈50 dB SMSR obtained with a two section DBR laser, proving that high-enough coupling coefficient is achievable with these shallow lateral gratings.

Although the SLG process is difficult to replicate with a planar UV-NIL patterning process ORC, has devised a process sequence for 'recessed gratings' that can be adapted to make this process UV-NIL-compatible. Unfortunately, there was not enough time to test the latest UV-NIL-compatible 'recessed gratings' process up to the point where a batch of devices could be fabricated with this approach.

LC-RWG surface gratings have also been fabricated deliberately exploiting the ARDE-induced trench width dependent etching rates to avoid footing problems. Fig. 2.4.2-4a shows a close view of the etch mask profile designed to avoid the un-etched pockets at the bottom of the grating shown for the 1st grating structure presented in the leftmost panels of Fig. 2.4.2-2.
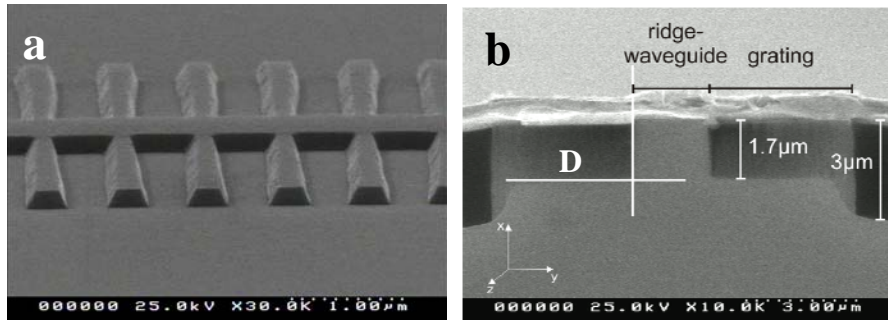

Fig. 2.4.2-4: (a) Etch mask profile designed to avoid ARDE-induced imperfect grating profiles; (b) cross section SEM image of a LC-RWG grating with extended lateral width and quasi-ideal grating profile.

Fig. 2.4.2-4b shows a cross section of a LC-RWG grating made by UWUERZ on a 1.3 µm legacy Fabry-Perot epiwafer from Modulight. Due the large lateral extension of the grating, D, the trench width dependent etching rates are largely avoided and nearly rectangular ridges have been obtained. This grating fabrication consists of one epitaxy and one lithography/etch step. No overgrowth and multiple etch steps are necessary. The DFB lasers employing these gratings show single mode behaviour with high side mode suppression values.

UKAS has developed a similar etch process for 1.55 µm, but with a much reduced lateral extension of the grating, D, to limit the lateral leakage current. Fig. 2.4.2-5a presents a focused ion beam (FIB) cut of a DFB laser with 2nd-order LC-RWG gratings. Due the ARDE-induced trench width dependent etching rates, the etch depth is reduced inside the trenches, leading to an imperfect triangular profile, which is used in the simulated mode profile of Fig. 2.4.2-5b. Nevertheless, the coupling strength was still large enough to achieve single longitudinal mode emission with SMSR >50 dB (as shown in Fig. 2.4.2-5c).
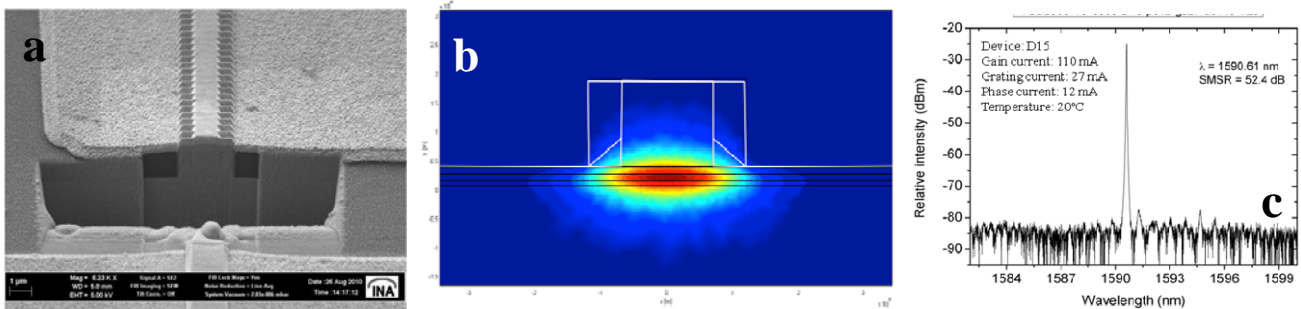

Fig. 2.4.2-5: (a) SEM view of the UKAS LC-RWG grating structure through a FIB cut of a DFB laser; (b) mode profile simulation taking into account the imperfect triangularly-shaped etching at the bottom of the LC-RWG grating; (c) single-mode emission spectrum of a three-section laser with such imperfect gratings, still exhibiting SMSR > 50 dB

2.4.3. Development of etched facets

The simulation studies have indicated that for increasing the yield of properly operating devices the reflection from at least one of the end facets should be as close as possible phase-matched with the grating reflections, mostly when the grating coupling coefficient is low. Since the position of the cleaved facets cannot be controlled precisely enough, ORC and UWUERZ have developed the fabrication of etched facets. Besides increasing the fabrication yield, the use of etched facets improves and stabilizes the characteristics of the lasers and eliminates the need of phase control in multi-section lasers.
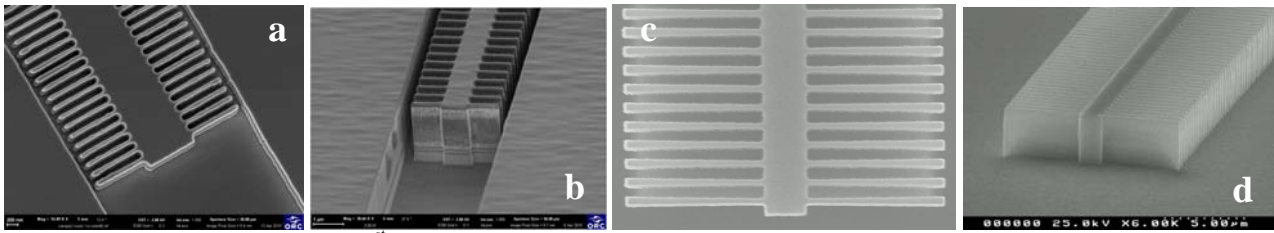
Fig. 2.4.3-1: (a) SEM top view for 1st-order grating etch mask imprinted using UV-NIL and (b) SEM view of the corresponding LC-RWG grating and etched facet fabricated at TTY-ORC; (c-d) top and 3D view of an LC-RWG grating and etched facet imprinted by EBL and fabricated by UWUERZ.

Fig. 2.4.3-1a shows the top view of the UV-NIL-imprinted etching mask for the end section of a laser with 1st-order LC-RWG gratings and an etched facet, while Fig. 2.4.3-1b shows the resulted grating and etched facet of the laser fabricated at ORC. While the gratings were etched only close to the waveguide layer, it can be observed from Fig. 2.4.3-1b that the etched facet was etched through the waveguide and active region. Similar views – top view of the etch mask and 3D view of the realized grating and etched facet – are given in Fig. 2.4.3-1c and 2.4.3-1d for a laser fabricated at UWUERZ. .

2.4.4. Newly developed high-aspect-ratio etching process

The fabrication of deeply-etched high-aspect-ratio gratings is difficult with the conventional one-step dry etch processes. UKAS has developed a new multi-step gas-chopping process consisting of etch, passivation and removal process steps, which can be repeated in several loops This process, developed for the InP based material system, allows an etch depth limited only by the resilience of the etch mask to the multi-step etching. Fig. 2.4.4-1, gives SEM pictures of etched lateral gratings obtained with 20 and 50 loops, reaching a record aspect ratio of 41. The scallops resulted from repeating the multi-step sequence are not affecting the side wall verticality. A patent application has been filled by UKAS for this new multi-step gas-chopping process.
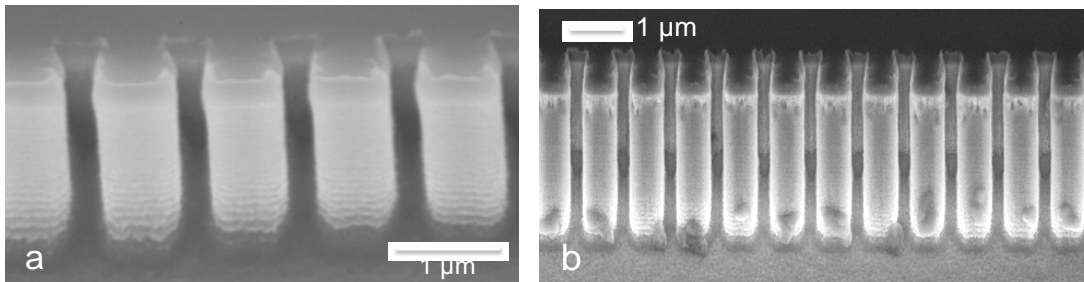
Fig. 2.4.4-1: (a) 1.7 μm deep gratings obtained with 20 loops having an etch step time of 55 sec. (b) 3.9 μm deep gratings, with a record-high aspect-ratio of more than 41, obtained with 50 loops having an etch step time of 55 sec.

2.4.5. Fabrication of single and multi-section DFB / DBR lasers

Single-section DFB lasers and multi-section DFB/DBR lasers have been processed, based on the different grating fabrication procedures described in the previous sections. A large part of these devices have been fabricated from legacy epiwafers, which were intended for Fabry-Perot lasers. Short cavity DFB lasers with cavity lengths below 300 μm were tested for their high-speed direct modulation capability but they did not achieve the target modulation bandwidths of the project. Multi-section devices, with up to 5 sections and several contact configurations, targeting extended direct modulation bandwidths by exploiting the PPR, were also fabricated using different grating fabrication procedures. Fig. 2.4.5-1a shows a schematic diagram of a 3-section CCIG laser, Fig. 2.4.5-1b gives a SEM view of the fabricated laser with electro-platted contact pads and Fig. 2.4.5-1c presents a magnified view of the grating onset, well aligned with the contact (the contact gap between sections is about 10 μm). Table 2.4.5-1 gives a summary of the main device variants that were investigated in the project. One important target of the project was to simplify the structure and the control (reduced number of contacts) for the lasers targeting enhanced direct modulation bandwidth by exploiting the PPR. The simplest laser structure which achieved PPR was a two-section DBR laser with shallow lateral gratings, fabricated by UKAS from epiwafers with two etch stop layers grown by III-V Lab. The device structure was fabricated according to a simplified design developed by PT, which employs only one DC-biased and directly-modulated section and one DC-biased phase-control section. The results obtained with this simplified laser structure are presented in the section dedicated to WP6.
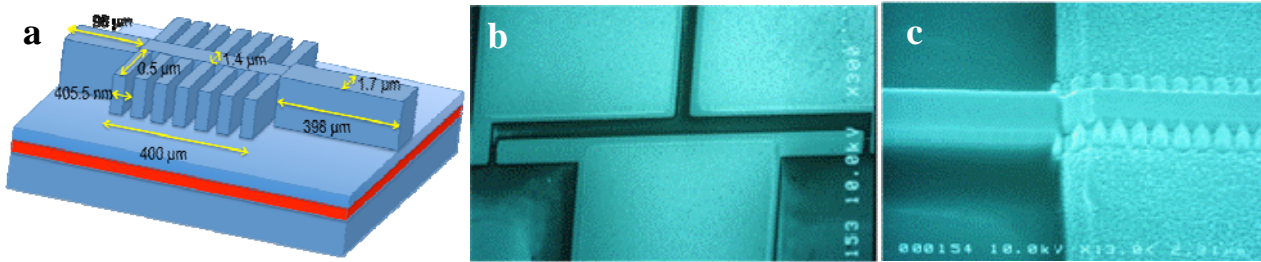
PUBLIC

24

Fig. 2.4.5-1: (a) Schematic diagram of a 3-section CCIG laser; (b) SEM view of the fabricated 3-section laser with electro-plated contact pads; (c) magnified view of the grating onset

Nr.	Laser structure	Design	Epiwafer	Processing (gratings / contacts)	Wave-length range	Main characteristics and observations
1	Single-section (short-cavity) DFB laser	TTY-ORC	InP-based, legacy FP, QW active region, from Modu	TTY-ORC & UWUERZ (LC-RWG / 1 contact)	1.3 μm	Small-signal (SS) modulation > 15 GHz but large signal (LS) modulation only up to 12-14 Gbit/s; inconclusive tests with etched facets and shorter cavities
2	Single-section QDash/QD lasers	UKAS	InP-based, new design, QDash and QD active region, from UKAS	UKAS (1 contact)	1.55 μm	Small-signal (SS) modulation only up to few GHz.
3	3-section CCIG lasers	PT	InP-based, new design, QW active region, from III-V Lab	UKAS (LC-RWG / 3 contacts)	1.55 μm	Technological control of cavity parameters not accurate enough to achieve PPR.
4	Dual-mode 3-section lasers	TTY-ORC	GaAs-based, new design, GaInAsN QW active region, from TTY-ORC	TTY-ORC (3 contacts)	1.3 μm	Losses too high for the requirements of lasers with enhanced modulation bandwidth by PPR.
5	Dual-mode 3-section lasers	TTY-ORC	InP-based, legacy FP, QW active region, from Modu and from III-V Lab	TTY-ORC & UWUERZ (LC-RWG / 3 contacts)	1.55 μm	PPR achieved consistently, -3 dB SS modulation bandwidth > 20 GHz but wrong contact structure and modulation scheme leads to large noise in small-signal (SS) modulation at low-frequency
6	Dual-mode 3-section lasers	TTY-ORC	InP-based, legacy FP, QW active region, from Modu	TTY-ORC UWUERZ (3 contacts, improved)	1.3 μm	PPR achieved consistently, improved modulation scheme eliminates SS modulation noise but LS modulation response limited to 14.5 Gbit/s due to strong PPR peak
7	Dual-mode 5-section lasers	TTY-ORC	InP-based, legacy FP, QW active region, from Modu	TTY-ORC (LC-RWG, 3, 5 contacts)	1.3 μm	PPR achieved consistently, relatively good SS modulation response, too low power due to imperfect realization
8	Two-section DBR laser	PT	InP-based, new design, QW active region, from III-V Lab	UKAS (SLG / 2, 3 contacts)	1.55 μm	Clear PPR, relatively flat SS modulation response, PPR-enhanced 21 GHz -3dB SS modulation bandwidth, no LS modulation consistent with project target
9	Single-section short-cavity QD laser	UKAS, TTY-ORC, TN	InP-based, new design, high-gain QD active region, from UKAS	UKAS (LC-RWG / 1 contact)	1.55 μm	15 Gbit/s LS modulation response extended to 23 Gbit/s after epilayer optimization (best results obtained after project end).

Table 2.4.5-1: Main laser structure variants investigated in the project
      (several batches with minor variations have been fabricated from each laser type)

2.5. Achievements in WP5 "Packaging and module development"

The main objectives of WP5 were:
- to complete a survey covering all the 100Gbit/s standardization activities;
- to search & test potential laser drivers for the high-speed laser diodes (LDs) developed in the project;
- to mount the DeLight LDs to ceramic (AlN) mounts for heat conducting and handling;
- to design and manufacture a single channel transmitter optical sub assembly (TOSA) supporting all laser drivers and laser diodes;
- to design and manufacture a TOSA host board capable to supply 3 independent bias current sources and one modulation AC signal; this board together with the driver board is attached to the TOSA;
- to design a printed circuit board (PCB) that has 3 independent 10-bit programmable current sources.

An additional task conducted by ColorChip was to integrate a single-section short-cavity DeLight LD into ColorChip's QSFP module and to test its eye diagram.

Following these objectives, the main scientific and technical results achieved in WP5 are:
- ✓ ColorChip made a survey for the next generation 100Gbps transceiver and found out that they will emerge to the telecom and data com market within 5 years while the market demands are indeed low-cost high-speed direct modulation laser diodes. This was exactly the research direction of DeLight consortium.
- ✓ ColorChip conducted several lab tests of laser drivers IC and found that current versions are suitable for EML (External Laser Modulation) up to ~50Gbps. ColorChip found that the current generation of high speed laser driver ICs are power consuming, while the emerging advanced ICs will consume less power, which is a vital demand for next generation high speed transceivers.
- ✓ ColorChip designed and tested controllable current sources for multiple-section high-speed directly-modulated lasers (DMLs).
- ✓ ColoChip designed and built a TOSA with the flexibility to test various single and multi-section structures and cavity lengths of direct modulation LDs fabricated by the DeLight consortium.
- ✓ ColorChip integrated a short cavity LD fabricated by the consortium into a QSFP transceiver and tested its eye quality. The measured rise time of 25ps is encouraging since it indicates that the laser large signal bandwidth is very large and within the DeLight objective.

2.5.1. Design of programmable triple current source

Some of DeLight laser diodes have 3 separate and independent sections, and none of the laser drivers that ColorChip have found have any support for DC current biasing 3 independent sections. Consequently, ColorChip designed, fabricated and tested a triple programmable current source. Fig. 2.5.1-1 gives the circuit schematic of one of the current sources and the PCB layout. The programmable triple current is connected and controlled by a PC using LabView software.
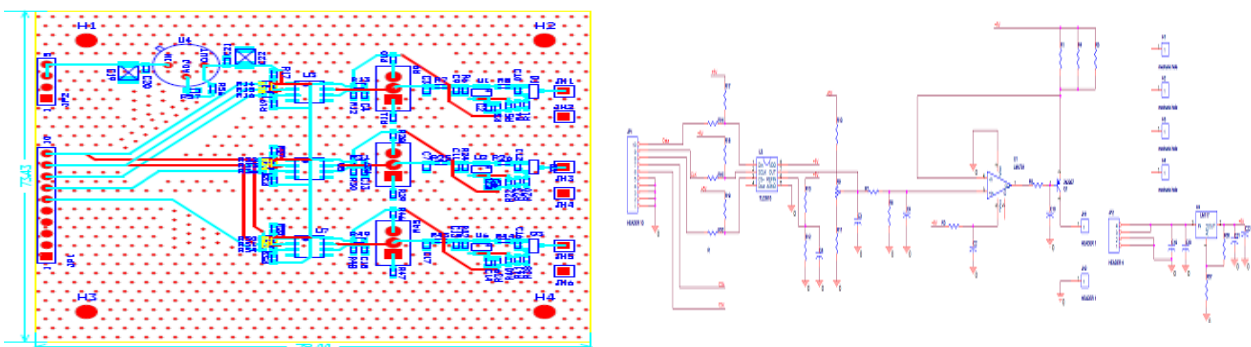
Fig. 2.5.1-1: Triple current source PCB design (left panel) and schematics of one channel out of three (right panel).

Each of the three current sources is connected by I2C (serial input) and is composed of 10bit DAC (Digital to Analog Convertor) buffered by an operational amplifier. A BJT transistor serves as a current source by simple voltage to current feedback circuit topology that converts DAC output voltage to current. The board was manufactured and tested. Fig. 2.5.1-2 shows a photograph of the board with components populated and a test characterization of one current source.
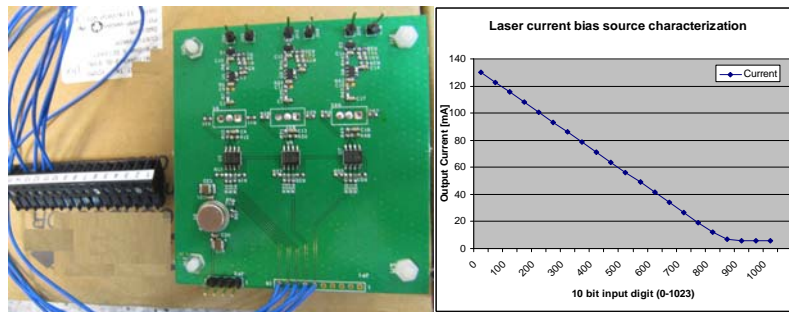
Fig. 2.5.1-2: A photograph of the triple current source board (left panel) and one current source characterization (right panel).

2.5.2. IC laser modulator drivers for 25/40G

One of ColorChip tasks was to find available chip vendors for laser drivers at 25/40Gbit/s and get some samples from them. Several high frequency ICs were found and evaluated. The 25/40Gbit/s ICs are not intended for direct laser current modulation but for driving laser modulators. They were designed for 50Ω impedance and not 5 to 10Ω laser diode impedance. The modulator drivers are basically wide bandwidth RF amplifiers having small input signal up to 40GHz and deliver large output signal to a 50Ω load. They are not programmable and not friendly to handle. This is in contrast to 10G mature technology laser drivers which supply not only the AC modulation current but also the DC bias current to the diode. In the 10G generation ICs, there is serial communication between a microcontroller that controls the entire module and the laser driver. The bias current and the modulation current are digitally programmable by the module's microcontroller. They also have automatic power control (APC) loop that changes automatically the laser bias current so that the output power will remain constant at all times. The 10G ICs work only with single voltage supply (3.3V) while the 25/40G ICs need several positive and negative voltages. The average power consumption of the laser modulators that ColorChip evaluated was about 1.5W. This power doesn't include the laser diode DC bias circuit. It should be noted that 4 drivers are needed for the 4x25=100Gbit/s transceiver, which will get the total power consumption to more than 6W.

Electrical tests were conducted, first at ColorChip with 12.5Gbit/s and later at Technion with 25Gbit/s (because ColorChip has measurement equipment only for frequencies up to 12.5Gbps). Fig. 2.5.2-1 shows the eye diagrams of the input and output signal at 12.5Gbps on the left and right panels, respectively, while Fig. 2.5.2-2 shows the eye diagrams of the input and output signal at 25Gbps on the left and right panels, respectively. The nice open and clear electrical eye at 25Gbps proves that the driver has the capability to drive the DeLight LDs at 25G and even more.
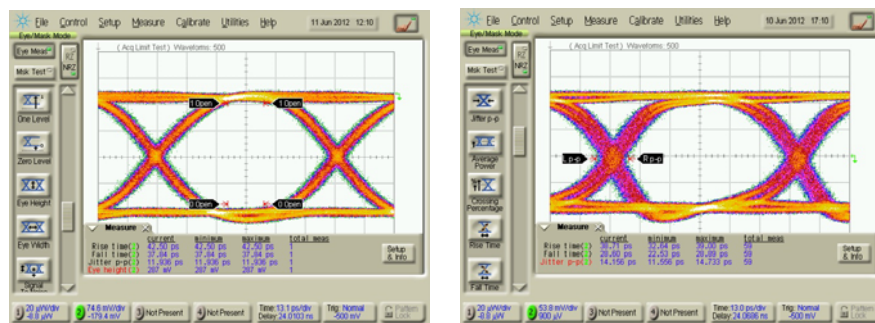

Fig. 2.5.2-1: Input and output eye diagrams at 12.5 Gbit/s (left and right panel, respectively).

Fig. 2.5.2-2: Input and output eye diagrams at 25 Gbit/s (left and right panel, respectively)

2.5.3. Design of TOSA Jig for single 25G laser diode

A special test bed (jig) was produced in order to connect the 25 Gbit/s signal to the LD, while biasing the diode with a triple DC current source. An aluminum base was designed and built by CNC machine. On this base, a small test PCB was designed and built. This test PCB is attached by screws and welded to the centre pin of SMA connector. The test PCB has a straight microstrip transmission line with 50Ω characteristic impedance coated with gold at the edges to enable wire bonding. Thus, it will be easy to wire bond the LD mounted close to the edge of the microstrip transmission line. The left panels of Fig. 2.5.3-1 depicts the setup of the jig and a 3-section LD. 3 printed inductors on the PCB isolate the AC signal from the 3 DC current sources.
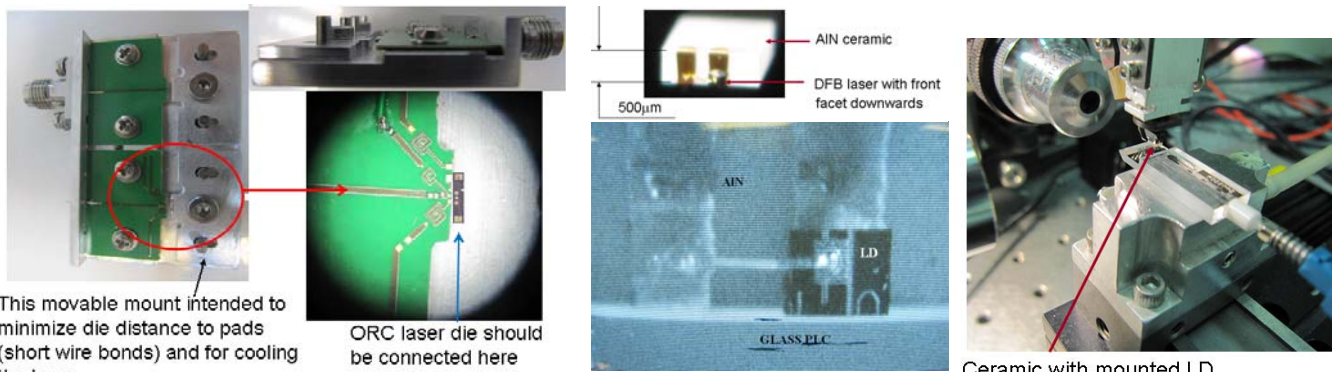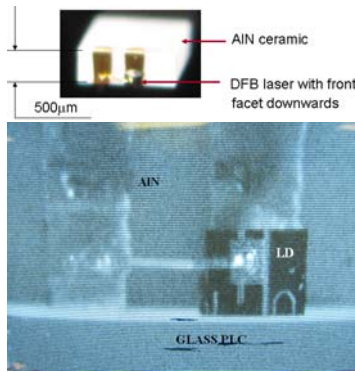

Fig. 2.5.3-1: Picture of the jig and a 3-section laser diode (two left panels); together with a picture of a short cavity DeLight DFB LD mounted on AlN (middle lower panel), which is actively attached on a PLC (right panel) and the picture of the LD wire bonded to the ceramic AIN and attached to the PLC (lower middle panel)

2.5.4. TOSA design based on ColorChip Propriety SystemOnGlass™

Short-cavity single-section DeLight LDs were integrated with ColorChip's proprietary technology for optical transceivers. An ORC DFB laser diode was mounted and wire bonded on an AlN submount. The ceramic submount was attached to a glass PLC and actively coupled to waveguide. This can be seen in the lower middle panel of Fig. 2.5.3-1. The PLC with the attached submount was assembled into QSFP transceiver module (as shown in Fig. 2.5.4-1) and tested.
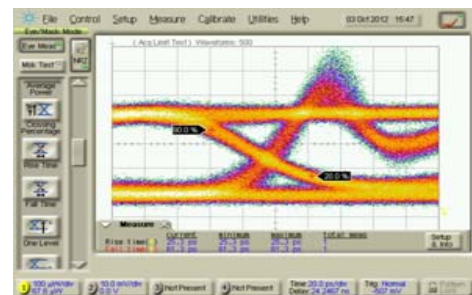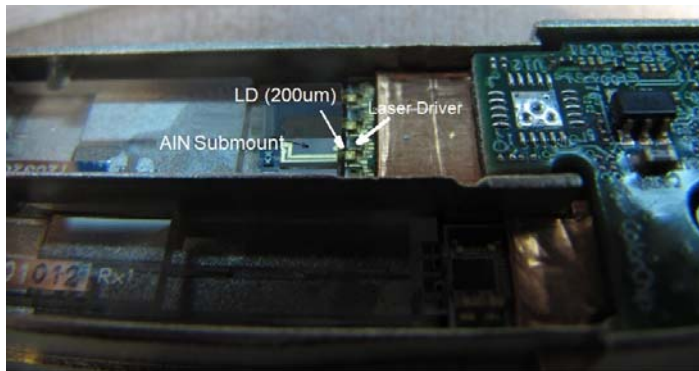
Fig. 2.5.4-1: The assembly of the PLC with ORC's short-cavity DFB laser inside standard QSFP (left panel) and measured 25 ps rise time of the optical signal (right panel)

The measured rise time of the optical signal was 25 ps, which was the same as the rise time of the laser driver itself. This means that the laser does not contribute additional delay and its rise time is very short (see the right panel of Fig. 2.5.4-1). The measurement of the optical signal was done without the internal filter of the scope, which artificially slows down the rise time of the signal.

2.6. Achievements in WP6 "Material, device and module characterization"

The main objectives of WP6 were:

- basic and microscopic characterization of standard and advanced laser gain material;
- in depth material characterization, focusing on optical transitions and carrier dynamics;
- small-signal modulation characterization, including noise characterization;
- large-signal modulation, noise and chirp characterization;
- reliability and lifetime characterization of laser chips;
- module and transmission system characterization.

Following these objectives, the main scientific and technical results achieved in WP6 are:

- ✓ basic and advanced thorough characterization of QD active regions, which enabled the analysis and optimization of QD growth conditions;
- ✓ small-signal and large-signal characterization of the fabricated lasers, which enabled parameter extraction as well as epilayer and device structure optimization;
- ✓ characterization of PPR, which enabled a better understanding of the PPR effects on small-signal and large-signal direct modulation;
- ✓ reliability and lifetest characterization, showing that, although new, the lasers with LC-RWG gratings and their fabrication procedures developed in the project have reliability and lifetime characteristics comparable with those achieved by the mature buried-grating structures and their fabrication technologies.

2.6.1. QD material characterization

Since the legacy epiwafers as well as most of the quantum well lasers were employing already thoroughly tested active region epilayer structures and epi-growth procedures, they did not require substantial material characterization efforts. Consequently, the material characterization, apart from the standard checking procedures, were concentrated on the GaInAsN dilute-nitride QW and InP-based quantum dot (QD) active regions, which were developed within the project. Material characterization took place at several partners, particularly where the epiwafers were grown and, supplementary, a substantial advanced QD material characterization effort was performed at WrUT. This has mainly concerned probing the optical properties of the active region by combining several spectroscopic techniques as modulation spectroscopy, photoluminescence, photoluminescence excitation and time-resolved measurements and the band structure calculations employing the multi-band k·p theory. Based on that, there could be derived such details of the novel active materials as the electronic structure, confined states levels and band gap discontinuities, optical material quality, radiative processes efficiency and main non-radiative recombination channels. And finally, the effect of temperature and polarization of the emission have been studied for all the materials. In case of quantum-dot-like active regions various structural morphologies and geometry modifications have been analyzed. Additionally, deep-level transient spectroscopy and time-resolved photoluminescence measurements were used to evaluate loss mechanisms more directly. Fig. 2.6-1 illustrates the improvement in QD size regularity achieved at UKAS in the early stages of the project by improved growth conditions resulted from microscopic and photoluminescence characterization.
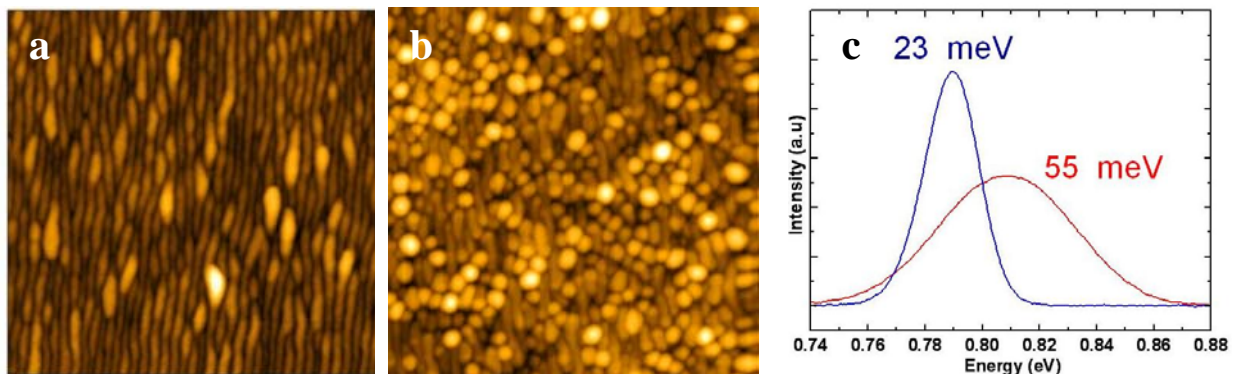
Fig. 2.6.1-1: (a) Atomic force microscopy (AFM) of QDs grown at UKAS in un-optimized As$_4$ growth mode as compared with (b) AFM of QDs grown on optimized As$_2$ growth mode together with (c) photoluminescence measurements showing narrower spectrum for the more uniform QDs grown under optimized conditions

Improved QD gain material was also characterized by atom probe tomography (APT) in a collaborative effort with the Fraunhofer Institute in Dresden. APT relies on forming (by focused ion beam) a sharp, needle like structure, placing it in a vacuum chamber where the combination of field emission, mass spectroscopy and a detailed computer analysis yield a three dimensional reconstruction of the chemical constituents of the material. A SEM view of an APT sample and the corresponding example result are given in Fig. 2.6.1-1.
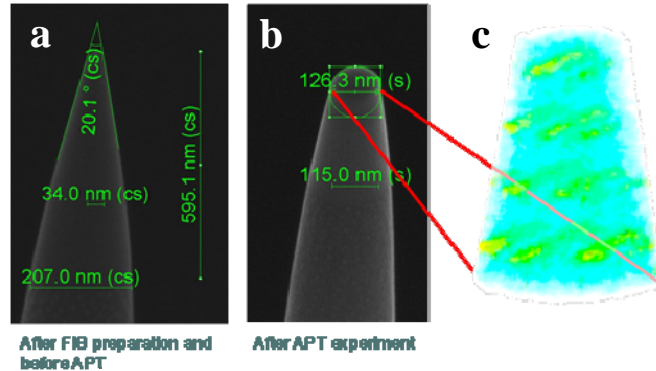

Fig. 2.6.1-2: APT sample structure (a) after FIB preparation and before APT and (b) after the APT experiment, together with (c) APT-determined 3D atomic distribution

By using the ATP data as well as high-resolution transmission electron microscopy (HRTEM) images obtained at TN, it was concluded that the newly developed dots are somewhat elongated but still offer three dimensional confinement as do perfectly round dots. WrUT developed a model for the polarization dependent emission and the exact energy levels of the dots, all consistent with experiments.

2.6.2. Device characterization

Basic device characterization took place mainly at the partners who fabricated the devices, while high-speed laser characterization was performed at Technion. Three types of lasers yielded relevant high-speed characterization results for PPR-enhanced modulation bandwidth. The first type is the multi-section dual-mode DFB lasers developed at ORC from legacy epiwafers provided by Modulight. Several generations of these lasers were fabricated, tested and characterized (the most important structures being given in Table 2.4.5-1). The experiments have confirmed that the dual-mode frequency spacing and, consequently, the PPR frequency can be largely determined by the longitudinal structure of the multi-section DFB lasers and dual-mode emission with frequency spacing ranging from 14 GHz to 1.3 THz have been obtained in good agreement with the simulations (see Fig. 2.2.4-2a, 2.2.4-2b and 2.6.2-1a). Also the intensity noise measurements confirmed that the dual-modes are quasi-phase-locked (see Fig. 2.2.4-2c). Unfortunately, the high-frequency PPR and/or the non-uniform small-signal modulation response (with a very pronounced PPR peak) led to relatively poor large-signal modulation (as explained by the Finite-Difference Travelling-Wave analysis exemplified in Fig. 2.2.4-4). Only 8 GHz small-signal modulation bandwidth and a large-signal modulation rate of 14.5 Gbit/s was achieved with these lasers, mainly due to the limited understanding of the PPR effects at the time of their design. The dual-mode lasers were, however, used in successful transmission experiments over 2 and 10 km, proving the transmission capability of these lasers for data-com distances.
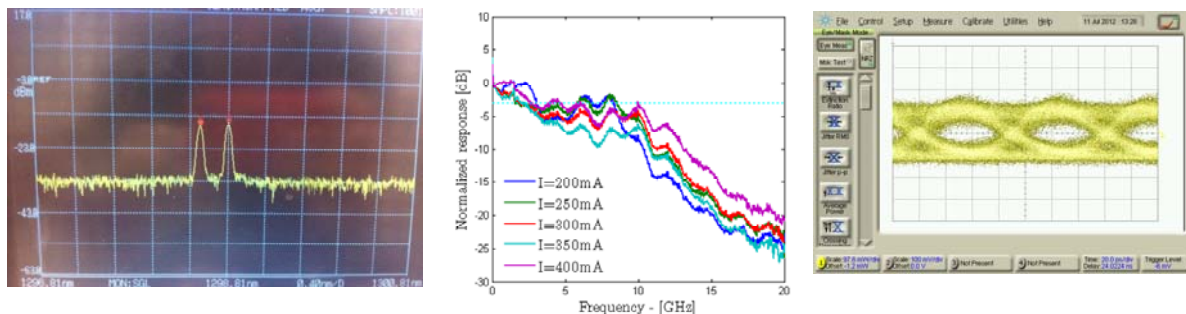
Fig. 2.6.2-1: (a) Measured dual-mode emission with frequency spacing determined by the laser structure in agreement with the design and simulations; (b) 8 GHz -3dB small-signal modulation bandwidth and (c) 14.5 Gbit/s large-signal eye diagrams at 14.5 Gbit/s for dual-mode multi-section DFB lasers

Taking into account the detrimental effects of a large dip between the CPR and PPR, we have studied the possibility to adjust the PPR position and the flatness of the modulation response between the CPR and PPR by adjusting the bias currents of the laser sections. Fig. 2.6.2-2a and 2.6.2-2b show the tuning of the PPR frequency (and the CPR changes) induced by adjusting one of the bias currents for a 1.6 mm long multi-section DFB laser emitting at 1.55 μm and for a 1.5 mm long multi-section DFB laser emitting at 1.3 μm, respectively. It can be observed how the CPR-PPR gap is filled when the PPR is brought closer to the CPR.
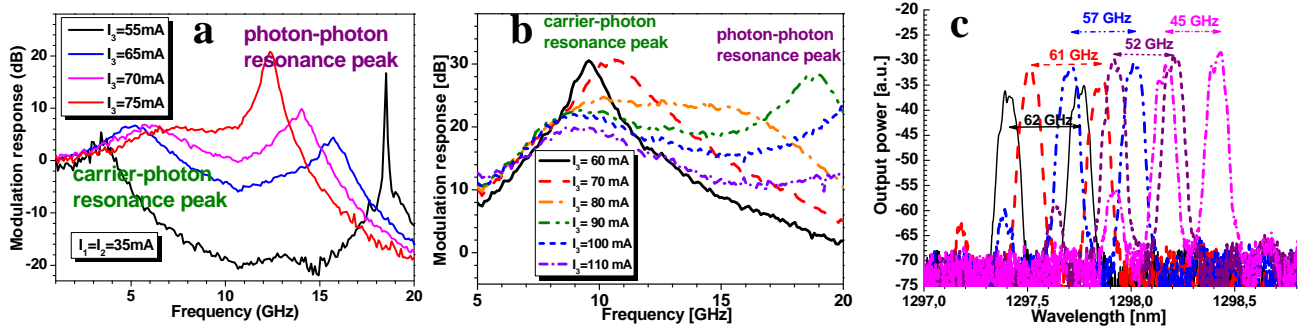

Fig. 2.6.2-2: Measured small-signal modulation response with the PPR position adjusted by the bias applied to one of the laser sections in: (a) 1.6 mm long multi-section laser with LC-RWG gratings emitting at 1.55 μm, (b) 1.5 mm long multi-section laser with LC-RWG gratings emitting at 1.3 μm; (c) difference frequency tuning by bias in dual-mode multi-section lasers.

Tuning the difference frequency in multi-section dual-mode lasers while also controlling the mode power balance (illustrated in Fig. 2.6.2-2c) can easily be accomplished in structures with separate contacts for the different sections (with the associated drawback of a more complex control).

An important virtue of the dual-mode multi-section lasers is their narrow linewidth, of the order of 250 KHz (see Fig. 2.6.2-3a), which is largely due to the long grating sections.
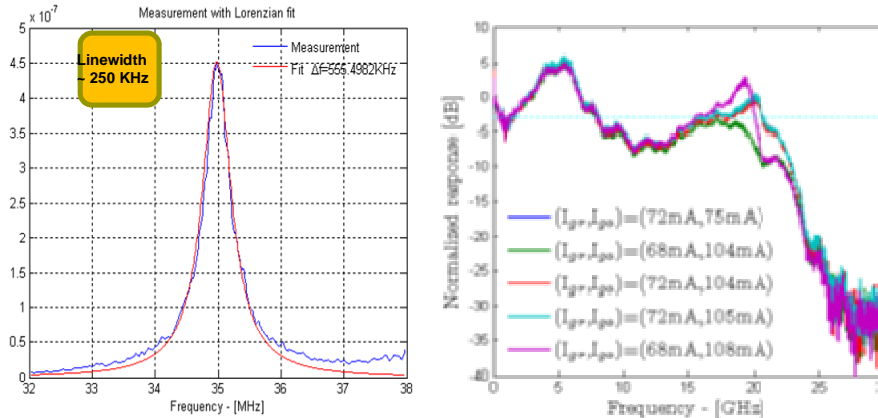

Fig. 2.6.2-3: (a) Measured and Voigt fit of 250 kHz linewidth for dual-mode lasers; (b) small-signal modulation response of multi-section DBR lasers at different bias combinations.

Another type of laser that achieved relevant results in extending the direct modulation bandwidth by exploiting the PPR is the multi-section DBR laser, designed by PT and processed at UKAS using InP-based 1550 nm epiwafers from III-V Lab. The basic structure of this laser is similar to a standard DBR laser except that the front gain section contained a short phase-control section. The exact lengths of the sections were carefully designed based on measured grating coupling coefficient values and the back facet of the LC-RWG grating section was AR coated. Fig. 2.6.2-3b shows a typical small-signal modulation response for these lasers, measured at TN. The small-signal modulation response exhibits a clear PPR peak, and this is actually the first ever observation of PPR in a two-section DBR laser. The response is rather flat, with a dip of less than 3 dB between the CPR and the PPR. For these lasers the small-signal modulation response is rather insensitive to the bias conditions (both gain and grating drive currents), which on one hand gives more stability to the device but on the other hand does not permit CPR-PPR dip adjustment and bias tuning of the PPR position.

The third laser type with significant high-speed modulation properties is the 1550 nm QD Fabry-Perot laser developed at UKAS. These QD lasers were tested dynamically in both the small and large signal regimes at temperatures ranging from 16 ^{0}C to 45 ^{0}C. The small signal responses are shown in Fig. 2.6.2-4. The

PUBLIC

31

bandwidth ranges from 8.3 GHz at 16 ^{0}C to 6.7 GHz at 45 ^{0}C. The bandwidth is rather insensitive to temperature changes as expected in QD lasers. The large signal responses at 20 ^{0}C for different bit rates are shown in Fig. 2.6.2-5. It should be underlined that in lasers where the modal gain, differential gain and nonlinear gain compression coefficient are all large the small signal response does not predict correctly digital modulation capabilities.
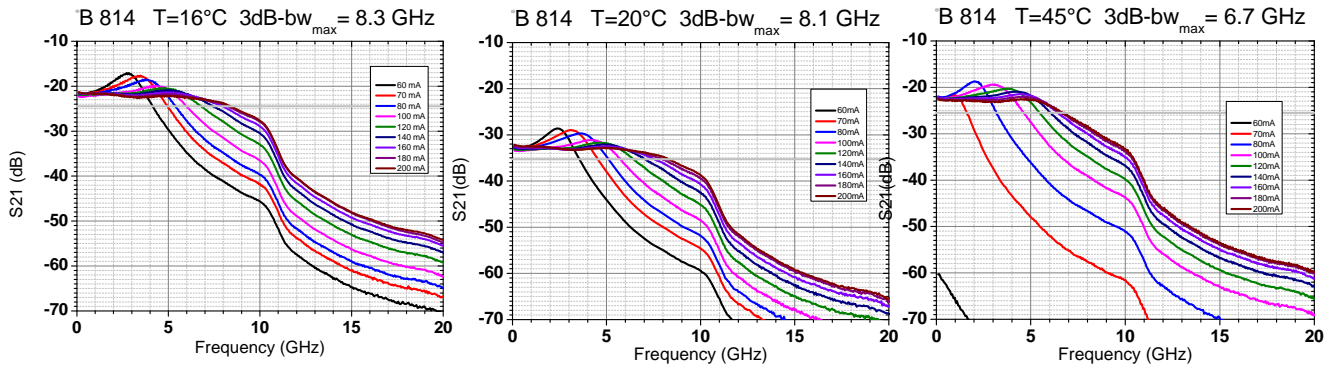

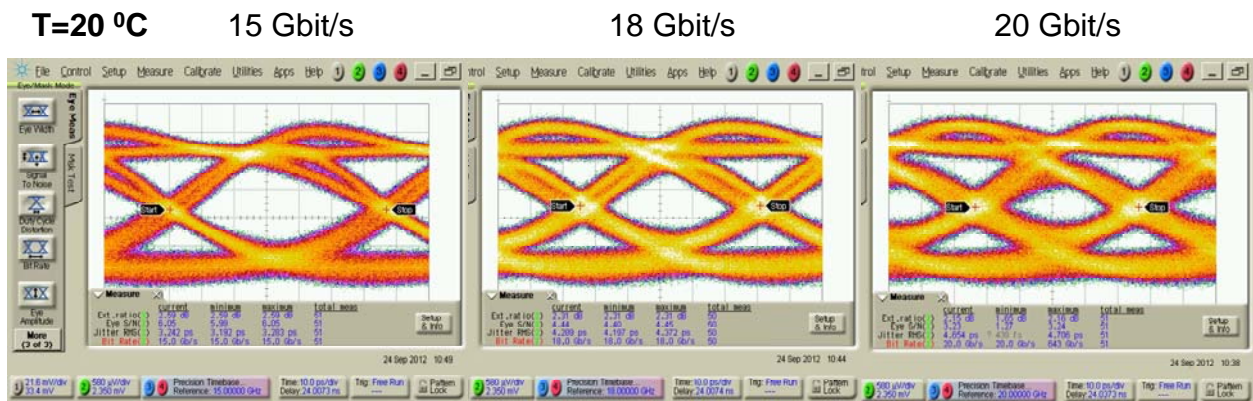**Fig. 2.6.2-4:** Small signal responses of the optimized 1550 nm QD laser

Fig. 2.6.2-5: Large signal responses of the optimized QD laser at 20 ^{0}C – different bit rates

Clear open eyes at 15 Gbit/s, 18 Gbit/s and 20 Gbit/s are observed in Fig. 2.6.2-5. These are the fastest responses ever recorded for an InP QD laser at 1550 nm. More of temperature-dependent large-signal responses at 20 Git/s are shown in Fig. 2.6.2-6. The responses are rather temperature independent in the range of 12 ^{0}C to 20 ^{0}C. This is partially due to the expected temperature insensitivity of QD lasers but also suggests that some limitation due to the packaging (mounting) affected the measurements. This means that the lasers are likely to be even faster than seen here.
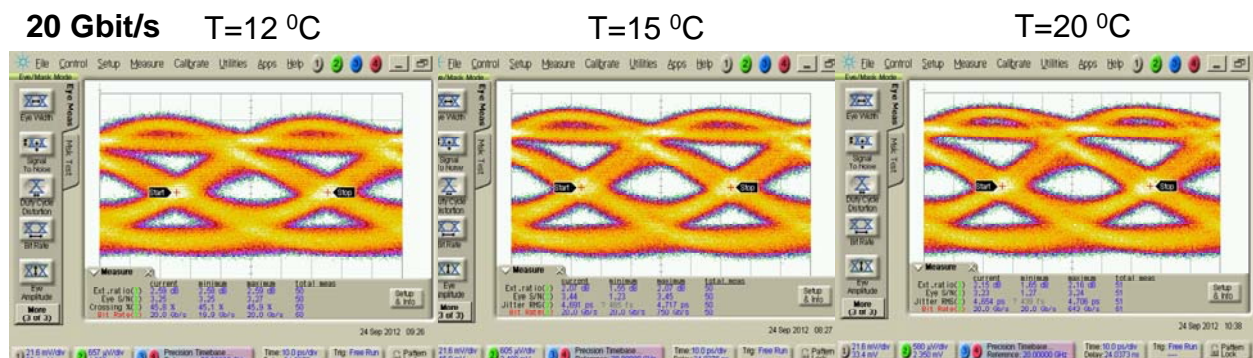

Fig. 2.6.2-6: 20 Gbit/s large-signal responses of the optimized QD laser at different temperatures

2.6.3. Reliability and lifetest of lasers with LC-RWG gratings

The reliability tests, which were started during the 2nd project period, were continued until the end of the project and even beyond. There were two types of DFB lasers in test: some with an older LC-RWG grating design (IDs 002/6/8) and some with an improved design (ID 017). The main purpose was to test the effect of surface gratings on the reliability. The material in use, AlGaInAs based 1550 nm structure, was selected because of availability of the DFB lasers early in the project and because it was known to have a good reliability as FP lasers, and therefore no material related degradation issues. The lasers were mounted p-up on heat sinks and tested with 5 mW operating power at 20°C temperature. The tests were run at the constant power mode so that the current was adjusted during the test. The operating current and voltage versus time are presented in Fig 2.6.3-1. The tests have been running for over 20000 hours and out of 10 devices three have failed at about 450 h, 2850 h and 3150 h. All the failed devices are with the older LC-RWG grating design. There is a clear variation in the operation of most diodes up to and at 1400 hours of testing. This is due to problems in the test system drivers that were repaired at that time. All the variation from the start of the test up to 1400 hours must therefore not be taken into account when evaluating the performance of the lasers. Otherwise the operation has been very stable with the exception of one laser of the improved design, 017-15, that has a sudden increase in the operating current and voltage at about 17500 hours, but even that laser becomes again stable after that for almost 3000 hours. Based on these tests it can be concluded that the LC-RWG surface gratings and their fabrication processes are not a source of additional reliability concerns.

1550 nm Surface Grating DFB Laser
APC Lifetest at 20°C
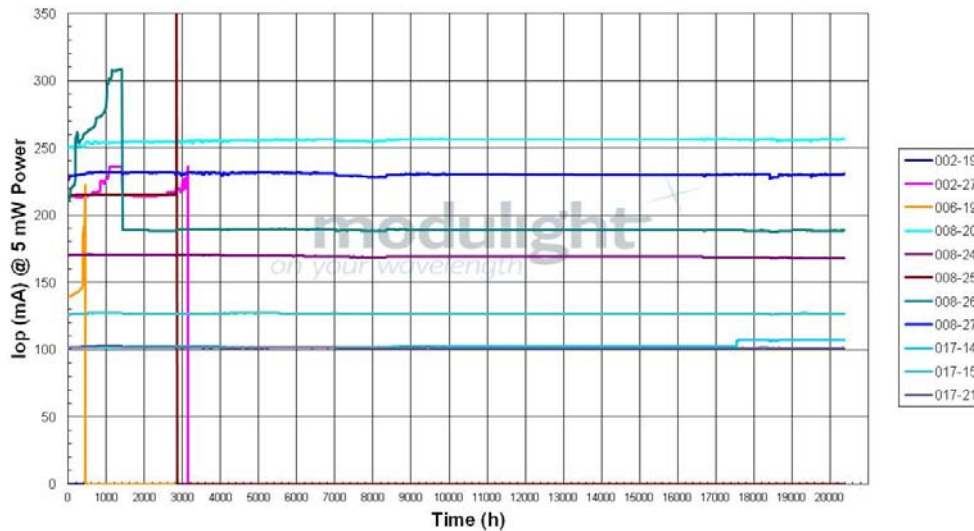
1550 nm Surface Grating DFB Laser
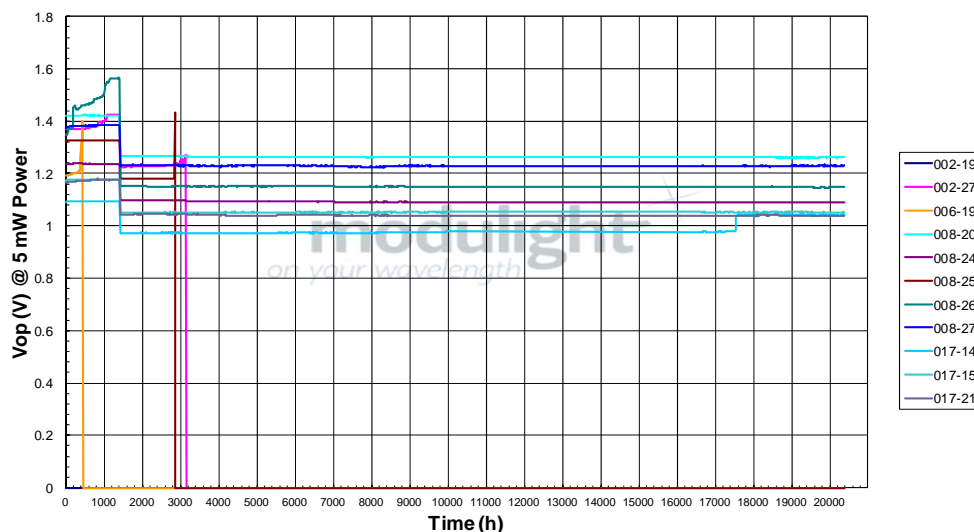**APC Lifetest at 20°C**

Fig. 2.6.3-1: Operating current (upper panel) and operating voltage (lower panel) vs. time for 1550 nm DFB lasers with older (002/6/8) and improved (017) LC-RWG grating designs.

2.7. Achievements in WP7 "Dissemination and exploitation"

The main objectives of WP7 were:
- to disseminate the project results in journals, conferences and public magazines
- to identify intellectual properties generated within the project and protect them
- to identify the current IPR situation and to evaluate the potential consequences for the use plan
- to survey the standardization activities and follow the market trends, preparing the exploitation of the project results.

Following these objectives, the main results achieved in WP7 are:
- ✓ 127 scientific/technical/technological contributions were published: 33 in peer review journals and 94 presented in international conferences;
- ✓ an international workshop on "High speed semiconductor lasers (HSSL)" was organized in Oct. 2010;
- ✓ the visibility of the project to the general public has been enhanced by the project WEB site (http://www.delightproject.eu/) and by articles in public magazines;
- ✓ a report on standardization activities was prepared, which includes the development decisions for the 100 Gbit Ethernet standard;
- ✓ 4 IPR items were identified and are filed as patent or in the process of patent application filing;
- ✓ a detailed technology implementation plan was prepared for the exploitation of project results.

The dissemination of the DeLight project results was carried out mainly by publishing papers in journals and by giving presentations at conferences (and publishing proceedings papers). The 127 scientific/technical/ technological contributions are listed in the Tables of section 4.1 and 4.2. They reflect most of the DeLight consortium achievements and concern all its activities, from modeling, simulation and analysis to device structure and new concept development and from technological optimization of the epitaxial growth and processing to advanced characterization results. Many papers have been published in well recognized and high rank journals as Applied Physics Letters, Photonics Technology Letters, Journal of Quantum Electronics, Journal of Selected Topics in Quantum Electronics, Electronics Letters, Physical Review B, and others. The results have also been presented at many of the most important events in the field of semiconductor lasers, low-dimensional structures and quantum electronics, as for instance: CLEO, ESLW, Photonics West, OECS 2011, IPRM, etc.

A website dedicated to the DeLight Project (www.delightproject.eu) has been maintained continuously though the entire project duration. The website put online the lists of journal papers presenting DeLight results (with the links to the article full texts on the journal websites) and the list of conference participations where DeLight results were presented. Additionally, the public part of the website contains the public deliverables of the project and the announcements and links to other dissemination events or press releases.

Many of the project achievements were also presented and amply discussed during the International Workshop on High Speed Semiconductor Lasers (HSSL) organized by the DeLight consortium, and held in Wroclaw, Poland, on 7-8 October 2010. A dedicated HSSL workshop website has been put up at www.delightproject.eu/hssl/. The workshop was a forum for the information and knowledge exchanges between the DeLight consortium and the most important other academic and industry-related institutions in the field of high speed lasers. 11 renowned experts from Europe, Japan and the United States were invited at the HSSL workshop, plus 15 contributed talks, some of them from DeLigh consortium partners.

Several other activities have been undertaken in order to make the information on DeLight available for a broader public audience. Several press releases introduced the project to a broader audience in the first two project years (HighTech Finland, 2009; Research Review Magazine 2009; European Optoelectronic Society myEOS.org in 2010) and an extensive article on the project achievements was published by the "Research Media Ltd." in their "International Innovation" magazine in April 2012.

3. General conclusions on the scientific and technical project outcome

(A) Modeling and simulation

The new or improved models (for the LC-RWG gratings, for the QD lasers, for the PPR) were extensively used in simulation studies and confirmed by experiments. The modeling and simulation results enabled better understanding of the physical phenomena and of the effects of technological limitations and supported the development of device structures and fabrication techniques. The following conclusion could be drawn:

- ✓ LC-RWG surface gratings can be a viable low-cost alternative to buried gratings, especially when very high coupling coefficients are not mandatory;
- ✓ the LC-RWG surface gratings can be applied successfully to most well-designed legacy epilayer structures intended for Fabry-Perot lasers;
- ✓ the PPR can be controlled systematically and reproducibly by laser structure (in several device configurations) and can be tuned by bias adjustments;
- ➢ the PPR can be exploited for extending the large-signal modulation bandwidth on condition that a relatively flat small-signal response over the -3dB bandwidth (with limited PPR peak) is obtained;
- ✓ the simulation studies indicate that data rates > 60 Gbit/s are feasible by PPR enhancement;
- ✓ QD lasers can be a competitive solution for high-speed direct modulation.

(B) Fabrication technology

The fabrication technology of surface defined gratings was widely investigated by different approaches (UV-NIL, e-beam based, different etching processes) and the following conclusions were drawn:

- ✓ UV-NIL is an effective low-cost high-throughput imprinting procedure down to sub-100 nm features;
- ✓ UV-NIL compatible fabrication processes for 1.3 and 1.5 µm DFB/DBR lasers with surface gratings have been clearly confirmed as a low-cost technological option;
- ✓ surface grating coupling coefficients in the $10 - 30$ cm^{-1} range can be achieved relatively easy with surface gratings but there are still substantial technological difficulties for achieving higher coupling coefficient values while maintaining low losses;
- ➢ the procedure(s) for the fabrication of lasers with surface gratings has to be further improved (especially with respect to fabrication yield) as expected for new fabrication processes applied to new structures).

(C) Bandwidth enhancement by exploiting the photon-photon-resonance effect

The concept of bandwidth enhancement by PPR was investigated by three major approaches (coupled-cavity injection lasers, multi-section DFB lasers and two-section DBR lasers) with the following results:

- ✓ the experiments have confirmed that the PPR frequency can be controlled by laser structure (at least in the multi-section DFB and two-section DBR laser configurations) and can be tuned by bias adjustments;
- ✓ substantial -3dB bandwidth enhancements can be obtained in the small signal response but those do not lead always to corresponding large-signal modulation bandwidths;
- ➢ large signal modulation and system experiments at 25 Gbit/s and beyond could not be demonstrated yet, due to remaining fabrication imperfections and lack of resources to solve these remaining problems within the project time and budget frame

(C) New quantum dot material development

The development of QD material for high-speed direct modulation led to the following conclusions:

- ✓ high modal gain QD active regions can be realized, which, in combination with optimized epilayer structures, allow data rates beyond 20 Gbit/s (the record value of 22 Gbit/s is more than two times higher than proposed at the beginning of the project);
- ✓ there is still a high potential to push the data rates achievable with QD lasers to even higher values;
- ➢ due to limitations in project resources short-cavity DFB lasers and two-section DBR lasers could not yet be tested with the advanced QD active regions.

(D) Market and standardization

The market and standardization surveys yielded the following conclusions:

- ✓ the DeLight objectives are addressing the demand for datacom applications on directly modulated low-cost lasers for 1.3 and 1.55 µm and DeLight goals are still 3-5 years ahead of the market;
- ✓ there are no driver electronics available on the market for >= 28 Gbit/s direct modulation;
- ✓ the DeLight lasers are compatible with commercial module subassemblies;
- ✓ there is no convincing solution currently on the market for the DeLight goals – DeLight is still unique.